

Post-Newtonian Orbital Effects Induced by the Mass Quadrupole and Spin Octupole Moments of an Axisymmetric Body

Lorenzo Iorio¹

¹Ministero dell' Istruzione e del Merito. Viale Unità di Italia 68, I-70125, Bari (BA), Italy

Abstract

The post-Newtonian orbital effects induced by the mass quadrupole and spin octupole moments of an isolated, oblate spheroid of constant density that is rigidly and uniformly rotating on the motion of a test particle are analytically worked out for an arbitrary orbital configuration and without any preferred orientation of the body's spin axis. The resulting expressions are specialized to the cases of (a) equatorial and (b) polar orbits. The opportunity offered by a hypothetical new spacecraft moving around Jupiter along a Juno-like highly elliptical, polar orbit to measure them is preliminarily studied. Although more difficult to be practically implemented, also the case of a less elliptical orbit is considered since it yields much larger figures for the relativistic effects of interest. The possibility of using the S stars orbiting the supermassive black hole in Sgr A* at the Galactic Center as probes to potentially constrain some parameters of the predicted extended mass distribution surrounding the hole by means of the aforementioned orbital effects is briefly examined.

Keywords: General relativity (641); Celestial mechanics (211); Planetary probes (1252)

1. Introduction

The most known post-Newtonian (pN) orbital effects, which have been extensively tested so far in different astronomical scenarios, are the gravitoelectric and gravitomagnetic precessions due to the mass monopole and the spin-dipole moments of the central body which acts as source of the gravitational field, respectively. The former is responsible for the well known, previously anomalous perihelion precession of Mercury in the Sun's field ([Le Verrier 1859](#)) of 42.98'' per century (arcsec cty^{-1}) ([Nobili and Will 1986](#)), whose explanation by [Einstein \(1915\)](#) was the first empirical success of his general theory of relativity (GTR). Such a feature of motion was later repeatedly measured with radar measurements of Mercury itself ([Shapiro et al. 1972](#); [Shapiro 1990](#)), of other inner planets ([Anderson et al. 1978, 1993](#)), and of the asteroid Icarus ([Shapiro et al. 1968, 1971](#)) as well. In more recent times, stars in the Galactic Center ([GRAVITY Collaboration et al. 2020](#)), binary pulsars ([Kramer et al. 2006](#)) and Earth's artificial satellites ([Lucchesi and Peron 2010, 2014](#)) were also used. The latter is the so-called Lense-Thirring effect ([Lense and Thirring 1918](#); [Mashhoon et al. 1984](#)), which is induced by the angular momentum of the central spinning body. It is currently being experimentally investigated around the Earth with the geodetic satellites of the LAGEOS family; see, for example, [Renzetti \(2013\)](#); [Iorio et al. \(2011\)](#); [Lucchesi et al. \(2020\)](#), and references therein. The gravitomagnetic precessions of the spins of some orbiting gyroscopes ([Pugh 1959](#); [Schiff 1960](#)) were detected in the field of the rotating Earth with the dedicated Gravity Probe B spaceborne mission ([Everitt 1974](#)) to a 19% accuracy level ([Everitt et al. 2011, 2015](#)), although the originally expected error was $\approx 1\%$ ([Everitt et al. 2001](#)).

Less known features of motion are the pN gravitoelectric and gravitomagnetic effects associated with the asphericity of a central body induced by its mass quadrupole and spin octupole moments, respectively ([Soffel et al. 1987](#); [Soffel 1989](#); [Heimberger et al. 1989](#); [Brumberg 1991](#); [Huang and Liu 1992](#); [Panhans and Soffel 2014](#); [Will 2014](#); [Iorio 2015](#); [Meichsner and Soffel 2015](#); [Frutos-Alfaro and Soffel 2018](#); [Schanner and Soffel 2018](#)). To date, they have never been measured; a detailed study for a proposed satellite-based mission in the field of the Earth, dubbed Highly Elliptical Relativity Orbiter, can be found in [Iorio \(2019c\)](#).

We will analytically work out, to the first pN (1pN) order, the net rates of change per orbit induced by the aforementioned departures from spherical symmetry of the source of the gravitational field without recurring to any simplifying assumption pertaining both the orbital configuration of the test particle and the orientation of the primary's spin axis in space. We will present

our results in a form that should make their interpretation and use in specific situations at hand simple and direct. Then, we will look at some astronomical scenarios that could be favorable for their measurement. Such a task would enlarge the empirical basis of GTR extending it to phenomena, although just in the 1pN regime, not yet tested. Conversely, they may provide further means to dynamically constrain, at least in principle, some key physical parameters of astronomical and astrophysical systems of interest. We will look neither at the directly measurable quantities in real spacecraft-based missions such as range and range rates, nor at the actual data reduction procedure (Moyer 2003). Instead, our goal is just to gain meaningful insights about the potential offered by the considered scenario(s) by performing a preliminary sensitivity analysis. To this aim, we will use the usual osculating Keplerian orbital elements (Soffel 1989; Brumberg 1991; Kopeikin et al. 2011; Soffel and Han 2019), which are easy to visualize in view of their clear geometric meaning.

The paper is organized as follows. In Section 2, the calculation scheme adopted to work out the long-term orbital features of motion under investigation is reviewed. The case of the pN gravitoelectric static field of a massive, oblate body is treated in Section 3, while the consequences of the gravitomagnetic spin octupole moment of a spinning primary is the subject of Section 4. Section 5 deals with some particular orbital configurations; in Section 5.1, the scenario where the satellite's orbital plane and the body's equatorial plane coincide (equatorial orbit) is considered, while Section 5.2 investigates the case where the orbital plane contains the body's spin axis (polar orbit). The results of Section 5.2 are applied in Section 6 to a Jovian scenario characterized by a putative spacecraft orbiting the fifth planet of our solar system along a highly elliptical polar orbit. A possible application of our results to the highly elliptical stellar motions in Sgr A* at the center of the Galaxy is outlined in Section 7. Section 8 summarizes our findings and offers concluding remarks. Appendix A contains a list of the symbols and definitions used throughout the paper.

2. Computational outline

The long-term orbital effects of interest are calculated by averaging over one satellite's orbital period the right-hand-sides of the equations for the variations of the Keplerian osculating elements in the Euler–Gauss form (Soffel 1989; Brumberg 1991; Kopeikin et al. 2011; Soffel and Han 2019)

$$\frac{da}{dt} = \frac{2}{n_b \sqrt{1-e^2}} \left[e A_R \sin f + \left(\frac{p}{r} \right) A_T \right], \quad (1)$$

$$\frac{de}{dt} = \frac{\sqrt{1-e^2}}{n_b a} \left\{ A_R \sin f + A_T \left[\cos f + \frac{1}{e} \left(1 - \frac{r}{a} \right) \right] \right\}, \quad (2)$$

$$\frac{dI}{dt} = \frac{1}{n_b a \sqrt{1-e^2}} A_N \left(\frac{r}{a} \right) \cos u, \quad (3)$$

$$\frac{d\Omega}{dt} = \frac{1}{n_b a \sin I \sqrt{1-e^2}} A_N \left(\frac{r}{a} \right) \sin u, \quad (4)$$

$$\frac{d\omega}{dt} = \frac{\sqrt{1-e^2}}{n_b a e} \left[-A_R \cos f + A_T \left(1 + \frac{r}{p} \right) \sin f \right] - \cos I \frac{d\Omega}{dt}, \quad (5)$$

$$\frac{d\eta}{dt} = -\frac{2}{n_b a} A_R \left(\frac{r}{a} \right) - \frac{(1-e^2)}{n_b a e} \left[-A_R \cos f + A_T \left(1 + \frac{r}{p} \right) \sin f \right], \quad (6)$$

evaluated onto the Keplerian ellipse

$$r = \frac{p}{1 + e \cos f}, \quad (7)$$

by means of

$$\frac{dt}{df} = \frac{r^2}{\sqrt{\mu p}}. \quad (8)$$

It turns out to be computationally convenient to express the position and velocity vectors as

$$\mathbf{r} = r (\hat{\mathbf{i}} \cos u + \hat{\mathbf{m}} \sin u), \quad (9)$$

$$\mathbf{v} = \sqrt{\frac{\mu}{p}} \left[-\hat{\mathbf{i}} (e \sin \omega + \sin u) + \hat{\mathbf{m}} (e \cos \omega + \cos u) \right]. \quad (10)$$

In the following, for the sake of simplicity, the angular brackets $\langle d\kappa/dt \rangle$ denoting the average over one orbital period of the rate of change of any one of the orbital elements κ will be omitted.

3. The 1pN acceleration induced by the oblateness of the central body

The pN gravitoelectric acceleration $\mathbf{A}_{\text{pN}}^{\text{obl}}$ experienced by a test particle orbiting an extended, oblate body is (Will 2014)

$$\mathbf{A}_{\text{pN}}^{\text{obl}} = \mathbf{A}^{\text{I}} + \mathbf{A}^{\text{II}} + \mathbf{A}^{\text{III}}, \quad (11)$$

where

$$\mathbf{A}^{\text{I}} = \frac{3 \mu J_2 R_c^2}{2 c^2 r^4} \left(v^2 - \frac{4 \mu}{r} \right) \left[(5 \xi^2 - 1) \hat{\mathbf{r}} - 2 \xi \hat{\mathbf{k}} \right], \quad (12)$$

$$\mathbf{A}^{\text{II}} = -\frac{6 \mu J_2 R_c^2}{c^2 r^4} \left[(5 \xi^2 - 1) v_r - 2 \xi \lambda \right] \mathbf{v}, \quad (13)$$

$$\mathbf{A}^{\text{III}} = -\frac{2 \mu^2 J_2 R_c^2}{c^2 r^5} (3 \xi^2 - 1) \hat{\mathbf{r}}. \quad (14)$$

$\mathbf{A}_{\text{pN}}^{\text{obl}}$ was derived earlier by Soffel et al. (1987); Soffel (1989); Brumberg (1991); Huang and Liu (1992) in a reference frame whose z -axis is aligned with $\hat{\mathbf{k}}$.

By following the computational scheme outlined in Section 2, one obtains the following expressions for the long-term rates of change of the Keplerian osculating elements induced by the sum of Equations (12)–(14).

$$\frac{da}{dt} = -\frac{9 e^2 (6 + e^2) n_b J_2 \mu R_c^2 (\widehat{T}_3 \sin 2\omega - 2 \widehat{T}_6 \cos 2\omega)}{8 c^2 a^2 (1 - e^2)^4}, \quad (15)$$

$$\frac{de}{dt} = -\frac{21 e (2 + e^2) n_b J_2 \mu R_c^2 (\widehat{T}_3 \sin 2\omega - 2 \widehat{T}_6 \cos 2\omega)}{16 c^2 a^3 (1 - e^2)^3}, \quad (16)$$

$$\frac{dI}{dt} = \frac{3 n_b J_2 \mu R_c^2 \left[\widehat{T}_4 (6 + e^2 \cos 2\omega) + e^2 \widehat{T}_5 \sin 2\omega \right]}{4 c^2 a^3 (1 - e^2)^3}, \quad (17)$$

$$\frac{d\Omega}{dt} = -\frac{3 n_b J_2 \mu R_c^2 \csc I \left[-e^2 \widehat{T}_4 \sin 2\omega + \widehat{T}_5 (-6 + e^2 \cos 2\omega) \right]}{4 c^2 a^3 (1 - e^2)^3}, \quad (18)$$

$$\begin{aligned} \frac{d\omega}{dt} = & -\frac{3 n_b J_2 \mu R_c^2}{16 c^2 a^3 (1 - e^2)^3} \left\{ (-8 + 3 e^2) (-2 \widehat{T}_1 + 3 \widehat{T}_2) + 14 \widehat{T}_3 \cos 2\omega + \right. \\ & \left. + 4 \left[e^2 \widehat{T}_4 \cot I \sin 2\omega + \widehat{T}_5 \cot I (6 - e^2 \cos 2\omega) + 7 \widehat{T}_6 \sin 2\omega \right] \right\}, \quad (19) \end{aligned}$$

$$\frac{d\eta}{dt} = \frac{n_b J_2 \mu R_c^2}{16 c^2 a^3 (1 - e^2)^{5/2}} \left[(80 + 73 e^2) (-2 \widehat{T}_1 + 3 \widehat{T}_2) + 42 (1 + 2 e^2) (\widehat{T}_3 \cos 2\omega + 2 \widehat{T}_6 \sin 2\omega) \right]. \quad (20)$$

The coefficients \widehat{T}_j , $j = 1, 2, \dots, 6$ are explicitly displayed in Appendix B. It should be remarked that Equations (15)–(20) are valid for any orbital configuration and for an arbitrary orientation of the body’s symmetry axis in space. They were calculated in Soffel et al. (1987); Brumberg (1991); Huang and Liu (1992) by orienting $\hat{\mathbf{k}}$ along the z axis of the reference frame chosen. Iorio (2015) worked out the pN oblateness-driven net shifts per orbit $\Delta\kappa$ of $\kappa = \{p, e, I, \Omega, \omega\}$ for an arbitrary orientation of $\hat{\mathbf{k}}$, but the resulting expressions are much more cumbersome than Equations (15)–(20) and a comparison with them is difficult.

The mixed effects due to the simultaneous presence of the 1pN gravitoelectric acceleration due to the mass monopole of the central body and the Newtonian acceleration induced by J_2 in the equations of motion (Heimberger et al. 1989; Huang and Liu 1992; Will 2014; Iorio 2015) will not be calculated here; they can be found, worked out in their full generality, in Iorio (2023). From an empirical point of view, it can be expected that they would affect post-fit residuals just with tiny mismodelled signatures since both the aforementioned accelerations are routinely modeled in any software used to reduce astronomical observations. In principle, also orbital variations of order $\mathcal{O}(J_2^2/c^2)$, arising from the mixed action of Equation (11) and the Newtonian oblateness-driven acceleration, should occur. Nonetheless, they are completely negligible since they would bring about in Equations (15)–(20) the scaling factor $J_2 (R_c/a)^2$.

4. The gravitomagnetic acceleration induced by the spin octupole moment of a rotating body

To the 1pN order, the gravitomagnetic Panhans-Soffel (PS) spin octupole¹ acceleration $\mathbf{A}_{\text{PS}}^{\text{oct}}$ experienced by a test particle orbiting an oblate spheroid of constant density that is rigidly and uniformly rotating is (Panhans and Soffel 2014)

$$\mathbf{A}_{\text{PS}}^{\text{oct}} = \frac{\mathbf{v}}{c^2} \times \mathbf{B}^{\text{oct}}, \quad (21)$$

where the gravitomagnetic field \mathbf{B}^{oct} can be calculated as Panhans and Soffel (2014)

$$\mathbf{B}^{\text{oct}} = -\nabla\phi^{\text{oct}}, \quad (22)$$

with the gravitomagnetic octupolar potential ϕ^{oct} given by Panhans and Soffel (2014)

$$\phi^{\text{oct}} = \frac{6 G S R_c^2 \varepsilon^2}{7 r^4} \mathcal{P}_3(\xi). \quad (23)$$

From Equations (21)–(23), the spin octupole PS acceleration can finally be cast into the form

$$\mathbf{A}_{\text{PS}}^{\text{oct}} = \frac{3 G S R_c^2 \varepsilon^2}{7 c^2 r^5} \mathbf{v} \times \left[5 \xi (7 \xi^2 - 3) \hat{\mathbf{r}} + 3 (1 - 5 \xi^2) \hat{\mathbf{k}} \right], \quad (24)$$

According to the computational scheme outlined in Section 2, the long-term rates of change of the osculating Keplerian orbital elements induced by Equation (24) turn out to be

$$\frac{da}{dt} = 0, \quad (25)$$

$$\frac{de}{dt} = \frac{45 e G S R_c^2 \varepsilon^2 (\hat{\mathbf{k}} \cdot \hat{\mathbf{h}}) (\widehat{T}_3 \sin 2\omega - 2 \widehat{T}_6 \cos 2\omega)}{28 c^2 a^5 (1 - e^2)^{5/2}}, \quad (26)$$

$$\begin{aligned} \frac{dI}{dt} = & -\frac{9 G S R_c^2 \varepsilon^2}{56 c^2 a^5 (1 - e^2)^{7/2}} \left(2(2 + 3e^2) (\hat{\mathbf{k}} \cdot \hat{\mathbf{l}}) (-4 \widehat{T}_1 + 5 \widehat{T}_2) + \right. \\ & \left. + 5 e^2 \left\{ (\hat{\mathbf{k}} \cdot \hat{\mathbf{l}}) \left[-2 \widehat{T}_1 + 3 (\hat{\mathbf{k}} \cdot \hat{\mathbf{l}})^2 + (\hat{\mathbf{k}} \cdot \hat{\mathbf{m}})^2 \right] \cos 2\omega + 2 (\hat{\mathbf{k}} \cdot \hat{\mathbf{m}}) \left[-\widehat{T}_1 + 2 (\hat{\mathbf{k}} \cdot \hat{\mathbf{l}})^2 + (\hat{\mathbf{k}} \cdot \hat{\mathbf{m}})^2 \right] \sin 2\omega \right\} \right), \quad (27) \end{aligned}$$

$$\frac{d\Omega}{dt} = -\frac{9 G S R_c^2 \varepsilon^2 \csc I}{56 c^2 a^5 (1 - e^2)^{7/2}} \left(2(2 + 3e^2) (\hat{\mathbf{k}} \cdot \hat{\mathbf{m}}) (-4 \widehat{T}_1 + 5 \widehat{T}_2) + \right.$$

¹The spin-dipole moment in Panhans and Soffel (2014) yields the usual Lense-Thirring acceleration (Petit and Luzum 2010). For other studies on relativistic multipoles, see, e.g., Meichsner and Soffel (2015); Schanner and Soffel (2018); Frutos-Alfaro and Soffel (2018).

$$+ 5 e^2 \left\{ -(\hat{\mathbf{k}} \cdot \hat{\mathbf{m}}) \left[-2 \widehat{T}_1 + (\hat{\mathbf{k}} \cdot \hat{\mathbf{l}})^2 + 3 (\hat{\mathbf{k}} \cdot \hat{\mathbf{m}})^2 \right] \cos 2\omega + 2 (\hat{\mathbf{k}} \cdot \hat{\mathbf{l}}) \left[-\widehat{T}_1 + (\hat{\mathbf{k}} \cdot \hat{\mathbf{l}})^2 + 2 (\hat{\mathbf{k}} \cdot \hat{\mathbf{m}})^2 \right] \sin 2\omega \right\}, \quad (28)$$

$$\begin{aligned} \frac{d\omega}{dt} = & \frac{9 G S R_c^2 \varepsilon^2}{56 c^2 a^5 (1 - e^2)^{7/2}} \left(4 (3 + 2 e^2) (\hat{\mathbf{k}} \cdot \hat{\mathbf{h}}) (-2 \widehat{T}_1 + 5 \widehat{T}_2) + \right. \\ & + 2 (2 + 3 e^2) (\hat{\mathbf{k}} \cdot \hat{\mathbf{m}}) (-4 \widehat{T}_1 + 5 \widehat{T}_2 \cot I) + 5 \left\{ 2 (1 + 2 e^2) (\hat{\mathbf{k}} \cdot \hat{\mathbf{h}}) \widehat{T}_3 - \right. \\ & - e^2 (\hat{\mathbf{k}} \cdot \hat{\mathbf{m}}) \left[-2 + (\hat{\mathbf{k}} \cdot \hat{\mathbf{l}})^2 + 3 (\hat{\mathbf{k}} \cdot \hat{\mathbf{m}})^2 \right] \cot I \left. \right\} \cos 2\omega + 10 (\hat{\mathbf{k}} \cdot \hat{\mathbf{l}}) \left\{ 2 (1 + 2 e^2) \widehat{T}_5 + \right. \\ & \left. + e^2 \left[-1 + (\hat{\mathbf{k}} \cdot \hat{\mathbf{l}})^2 + 2 (\hat{\mathbf{k}} \cdot \hat{\mathbf{m}})^2 \right] \cot I \right\} \sin 2\omega \Big), \quad (29) \end{aligned}$$

$$\frac{d\eta}{dt} = -\frac{9 G S R_c^2 \varepsilon^2 (\hat{\mathbf{k}} \cdot \hat{\mathbf{h}})}{28 c^2 a^5 (1 - e^2)^2} \left\{ 5 \widehat{T}_3 \cos 2\omega + 2 \left[-2 \widehat{T}_1 + 5 (\widehat{T}_2 + \widehat{T}_6 \sin 2\omega) \right] \right\}. \quad (30)$$

It must be remarked that Equations (25)–(30) retain their validity for any orientation of $\hat{\mathbf{k}}$ in space, and for arbitrary orbital configurations. The gravitomagnetic spin octupole orbital precessions were explicitly calculated by Iorio (2019a,b) in the special case of $\hat{\mathbf{k}}$ aligned with the z axis of the reference frame adopted. In fact, also general formulas for them, valid for arbitrary orbital geometries and orientations of $\hat{\mathbf{k}}$ in space, were obtained by Iorio (2019a,b); nonetheless, they are much more cumbersome and less compact than Equations (25)–(30), so that a straightforward comparison is difficult. The interplay of the Newtonian acceleration due to J_2 and the pN one of Equation (24) would induce, in principle, mixed effects of order $\mathcal{O}(S \varepsilon^2 J_2/c^2)$. Nonetheless, also in this case, they would be negligible because of the multiplicative factor $J_2 (R_c/a)^2$ by which Equations (25)–(30) would be scaled down.

5. Some special orbital configurations

Here, two particular orbital configurations are considered: (a) equatorial (Section 5.1) and (b) polar (Section 5.2) orbits. By parameterizing $\hat{\mathbf{k}}$ in terms of the polar angles² α , δ as in Appendix A, one has

$$\hat{\mathbf{k}} \cdot \hat{\mathbf{l}} = \cos \delta \cos (\alpha - \Omega), \quad (31)$$

$$\hat{\mathbf{k}} \cdot \hat{\mathbf{m}} = \sin I \sin \delta + \cos I \cos \delta \sin (\alpha - \Omega), \quad (32)$$

$$\hat{\mathbf{k}} \cdot \hat{\mathbf{h}} = \cos I \sin \delta - \sin I \cos \delta \sin (\alpha - \Omega). \quad (33)$$

5.1. Equatorial orbit

Let us assume that the satellite's orbital plane coincides with the body's equatorial plane, irrespectively of the orientation of the latter in the adopted reference frame, i.e., for generic values of α , δ : it is

$$\hat{\mathbf{k}} \cdot \hat{\mathbf{l}} = \hat{\mathbf{k}} \cdot \hat{\mathbf{m}} = 0, \quad (34)$$

$$\hat{\mathbf{k}} \cdot \hat{\mathbf{h}} = 1. \quad (35)$$

According to Equations (31)–(33), the conditions of Equations (34)–(35) are fulfilled for

$$I = -\delta + \frac{\pi}{2}, \quad (36)$$

²If referred to the International Celestial Reference Frame (ICRF), α and δ are the R.A. and decl. of the primary's north pole of rotation, respectively (Seidelmann et al. 2007).

$$\Omega = \alpha + \frac{\pi}{2}. \quad (37)$$

Then, Equations (15)–(20) reduce to

$$\frac{da}{dt} = 0, \quad (38)$$

$$\frac{de}{dt} = 0, \quad (39)$$

$$\frac{dI}{dt} = 0, \quad (40)$$

$$\frac{d\Omega}{dt} = 0, \quad (41)$$

$$\frac{d\omega}{dt} = -\frac{3 n_b J_2 \mu R_c^2 (8 - 3 e^2)}{8 c^2 a^3 (1 - e^2)^3}, \quad (42)$$

$$\frac{d\eta}{dt} = -\frac{n_b J_2 \mu R_c^2 (80 + 73 e^2)}{8 c^2 a^3 (1 - e^2)^{5/2}}, \quad (43)$$

while Equations (25)–(30) can be written as

$$\frac{da}{dt} = 0, \quad (44)$$

$$\frac{de}{dt} = 0, \quad (45)$$

$$\frac{dI}{dt} = 0, \quad (46)$$

$$\frac{d\Omega}{dt} = 0, \quad (47)$$

$$\frac{d\omega}{dt} = -\frac{9 G S R_c^2 \varepsilon^2 (3 + 2 e^2)}{7 c^2 a^5 (1 - e^2)^{7/2}}, \quad (48)$$

$$\frac{d\eta}{dt} = \frac{9 G S R_c^2 \varepsilon^2}{7 c^2 a^5 (1 - e^2)^2}. \quad (49)$$

Note that Equations (42)–(43) and Equations (48)–(49) describe genuine secular trends.

5.2. Polar orbit

Let us assume that the body's spin axis, irrespectively of its orientation in the adopted coordinate system, i.e., for generic values of α , δ , lies somewhere in the satellite's orbital plane between $\hat{\mathbf{i}}$ and $\hat{\mathbf{m}}$. Such an orbital geometry is widely adopted in

spacecraft-based missions to solar system planets like, e.g., Juno at Jupiter (Bolton et al. 2017). In such a scenario, it is

$$\hat{\mathbf{k}} \cdot \hat{\mathbf{I}} \neq 0, \quad (50)$$

$$\hat{\mathbf{k}} \cdot \hat{\mathbf{m}} \neq 0, \quad (51)$$

$$\hat{\mathbf{k}} \cdot \hat{\mathbf{h}} = 0. \quad (52)$$

Equation (52) implies that the orbital angular momentum is perpendicular to the body's spin axis. Equations (31)–(33) tell us that the conditions of Equations (50)–(52) are satisfied for

$$I = \frac{\pi}{2}, \quad (53)$$

$$\Omega = \alpha; \quad (54)$$

indeed, with Equations (53)–(54), one has just

$$\hat{\mathbf{k}} \cdot \hat{\mathbf{I}} = \cos \delta, \quad (55)$$

$$\hat{\mathbf{k}} \cdot \hat{\mathbf{m}} = \sin \delta, \quad (56)$$

$$\hat{\mathbf{k}} \cdot \hat{\mathbf{h}} = 0. \quad (57)$$

As a consequence, Equations (15)–(30) reduce to

$$\frac{da}{dt} = \frac{9 e^2 (6 + e^2) n_b J_2 \mu R_c^2 \sin [2 (\delta - \omega)]}{8 c^2 a^2 (1 - e^2)^4}, \quad (58)$$

$$\frac{de}{dt} = \frac{21 e (2 + e^2) n_b J_2 \mu R_c^2 \sin [2 (\delta - \omega)]}{16 c^2 a^3 (1 - e^2)^3}, \quad (59)$$

$$\frac{dI}{dt} = 0, \quad (60)$$

$$\frac{d\Omega}{dt} = 0, \quad (61)$$

$$\frac{d\omega}{dt} = -\frac{3 n_b J_2 \mu R_c^2 \{-8 + 3 e^2 + 14 \cos [2 (\delta - \omega)]\}}{16 c^2 a^3 (1 - e^2)^3}, \quad (62)$$

$$\frac{d\eta}{dt} = \frac{n_b J_2 \mu R_c^2 \{80 + 73 e^2 + 42 (1 + 2 e^2) \cos [2 (\delta - \omega)]\}}{16 c^2 a^3 (1 - e^2)^{5/2}}, \quad (63)$$

while Equations (25)–(30) become

$$\frac{da}{dt} = 0, \quad (64)$$

$$\frac{de}{dt} = 0, \quad (65)$$

$$\frac{dI}{dt} = -\frac{9 G S R_c^2 \varepsilon^2 \cos \delta \{4 + 6 e^2 + 5 e^2 \cos [2(\delta - \omega)]\}}{56 c^2 a^5 (1 - e^2)^{7/2}}, \quad (66)$$

$$\frac{d\Omega}{dt} = -\frac{9 G S R_c^2 \varepsilon^2 \sin \delta \{4 + 6 e^2 + 5 e^2 \cos [2(\delta - \omega)]\}}{56 c^2 a^5 (1 - e^2)^{7/2}}, \quad (67)$$

$$\frac{d\omega}{dt} = 0, \quad (68)$$

$$\frac{d\eta}{dt} = 0. \quad (69)$$

Equations (58)–(59), Equations (62)–(63), and Equations (66)–(67), in addition to secular trends, when present, include also long-period signatures due to the evolution of pericentre which is mainly driven by the zonal harmonics of the Newtonian component of the multipolar field of the central body (Capderou 2005).

It can be shown that, for the orbital configuration of Equations (53)–(54), the classical precessions of I and Ω due to the zonal harmonics of the primary's gravitational potential vanish; see Appendix A of Iorio et al. (2023). It is important since such classical effects are usually regarded as a major source of systematic bias in assessing the error budget of a mission dedicated to measure certain general relativistic features of motion.

On the other hand, Equation (15) has not a classical counterpart acting as a systematic bias: it is true for any orbital configuration and primary's spin axis orientation, being the Newtonian oblateness-driven rate of change of a exactly zero. As far as the eccentricity is concerned, in general, the odd zonal harmonics of the classical gravity field of the source induce net variations per orbit which do not vanish for the polar geometry of Equations (53)–(54). It turns out that they are harmonic signatures oscillating with odd multiples of the pericentre frequency, while Equation (59) varies just at twice the frequency of ω . More specifically, by following the approach outlined in Appendix A of Iorio et al. (2023), one has

$$\dot{e}^{(J_3)} = \frac{3 n_b R_c^3 J_3 \sin(\delta - \omega)}{8 a^3 (1 - e^2)^2}, \quad (70)$$

$$\dot{e}^{(J_5)} = \frac{15 n_b R_c^5 J_5 \{8 + 13 e^2 + 14 e^2 \cos [2(\delta - \omega)]\} \sin(\delta - \omega)}{256 a^5 (1 - e^2)^4}, \quad (71)$$

$$\dot{e}^{(J_7)} = \frac{105 n_b R_c^7 J_7 \{40 + 208 e^2 + 82 e^4 + 6 e^2 (36 + 19 e^2) \cos [2(\delta - \omega)] + 33 e^4 \cos [4(\delta - \omega)]\} \sin(\delta - \omega)}{8192 a^7 (1 - e^2)^6}, \quad (72)$$

and so on. Either the even and the odd zonals make the pericentre to vary, as per Equations (A10) to (A16) of Iorio et al. (2023). Furthermore, if the condition

$$\omega = \delta - \frac{\pi}{2} \quad (73)$$

is selected, it turns out that the pericentre precessions due to the odd zonals vanish (Iorio et al. 2023). On the other hand, if the condition of Equation (73) holds, Equations (58)–(59) vanish as well.

6. The Jovian scenario for a dedicated mission

In view of its size, Jupiter, whose relevant physical parameters are listed in Table 1, seems to be the ideal³ candidate, at least in principle, to try to measure the general relativistic effects treated in the previous sections with a dedicated spacecraft-based

³The fifth planet of our solar system was often been considered for testing various aspects of gravitomagnetism over the years; see, e.g., Haas and Ross (1975); Mashhoon (2000); Tartaglia (2000b,a); Iorio (2010); Schäfer et al. (2017); Iorio (2019a).

mission. With a pinch of irony, we preliminarily dub it IORIO, acronym of In-Orbit Relativity Iuppiter⁴ Observatory, or, equally well, of IOvis⁵ Relativity In-orbit Observatory (Iorio 2019a,b). Moreover, both for typical planetological goals⁶ and to preserve

Table 1. Relevant physical parameters of Jupiter (Soffel et al. 2003; Seidelmann et al. 2007; Petit and Luzum 2010; Iess et al. 2018).

Parameter	Units	Numerical Value
μ	$\text{m}^3 \text{s}^{-2}$	1.26713×10^{17} (Petit and Luzum 2010)
J_2	$\times 10^{-6}$	14696.572 (Iess et al. 2018)
J_3	$\times 10^{-6}$	-0.042 (Iess et al. 2018)
S	$\text{kg m}^2 \text{s}^{-1}$	6.9×10^{38} (Soffel et al. 2003)
α	deg	268.057132 (Iess et al. 2018)
δ	deg	64.497159 (Iess et al. 2018)
R_e	km	71492 (Seidelmann et al. 2007)
R_p	km	66854 (Seidelmann et al. 2007)
ε	–	0.354

the onboard scientific instrumentation from harmful radiation⁷, the orbits of the spacecraft targeted to the fifth planet of our solar system are usually just polar and widely elliptical; thus, we can rely upon the results of Section 5.2. A notable existing example of such a peculiar orbital geometry is provided by the ongoing mission Juno (Bolton et al. 2017). It is currently orbiting Jupiter along a wide 53 days orbit characterized by a pericenter height of

$$h_{\text{peri}} = 4200 \text{ km} \quad (74)$$

and an apocenter height of

$$h_{\text{apo}} = 8.1 \times 10^6 \text{ km}, \quad (75)$$

corresponding to a semimajor axis

$$a = 4.1 \times 10^6 \text{ km} = 57.7 R_e \quad (76)$$

and an eccentricity

$$e = 0.981. \quad (77)$$

Originally, a 13 days orbit, corresponding to a lower apocenter height of

$$h_{\text{apo}} = 3.2 \times 10^6 \text{ km}, \quad (78)$$

and eccentricity

$$e = 0.954 \quad (79)$$

was planned for Juno (Matousek 2007), but problems with two helium valves in its propulsion system in 2016 October prevented to meet such a goal⁸.

For the sake of concreteness, in the following we will consider a putative spacecraft having the same pericenter height as Juno, given by Equation (74), while its apocenter height is allowed to vary from, say,

$$h_{\text{apo}} = 1.5 \times 10^6 \text{ km} \quad (80)$$

to the current Juno value of Equation (75), corresponding to a range variation for e of $\simeq 0.92 - 0.98$. Obtaining Equation (80) would be a demanding task since more fuel would be needed, and the spacecraft would be exposed to a larger amount of radiation.

⁴ *Iuppit̄er* is one of the forms of the Latin noun of the god Jupiter.

⁵ In Latin, *Iōvis* means “of Jupiter”.

⁶ Polar orbits, taking the spacecraft over the poles of the planet, allow the probe to traverse the latter in a north–south direction; they are optimal for mapping and monitoring it (Montenbruck and Gill 2000).

⁷ Radiation belts are the regions of a magnetosphere where high energy charged particles, such as electrons, protons, and heavier ions, are trapped in large amounts. All planets in our solar system having a sufficiently intense magnetic field, such as Earth, Jupiter, Saturn, Uranus, and Neptune, host radiation belts (Mauk and Fox 2010; Mauk 2014). Jupiter has the most complex and energetic radiation belts in our solar system and one of the most challenging space environments to measure and characterize in-depth (Roussos et al. 2022).

⁸ See <https://www.science.org/content/article/avoid-risk-misfire-nasas-juno-probe-will-keep-its-distance-jupiter>.

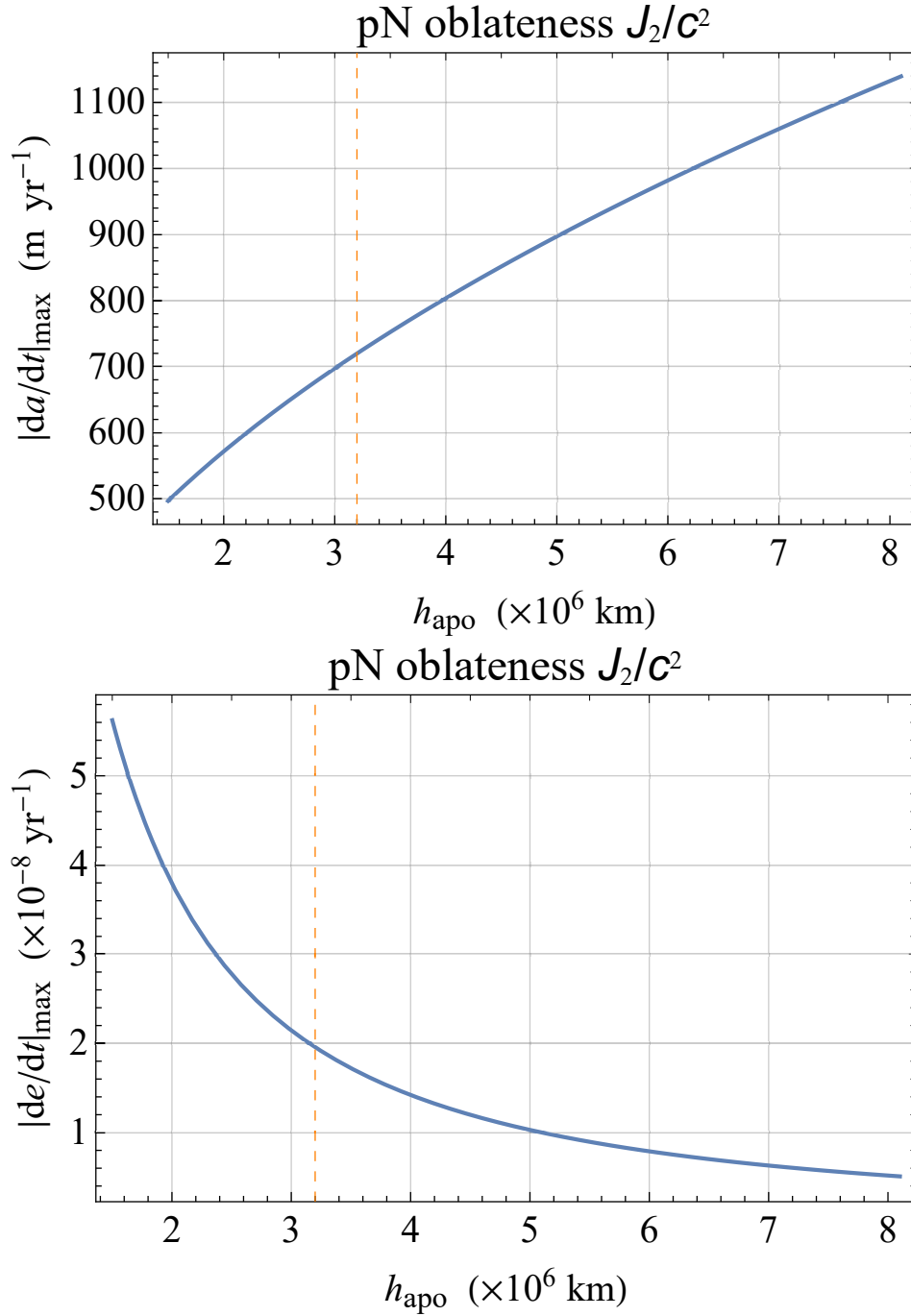


Figure 1. Plot of the amplitudes, in m yr^{-1} and 10^{-8} yr^{-1} , respectively, of Equations (58)–(59), calculated for the polar orbital configuration of Equations (53)–(54), as functions of the apocenter height h_{apo} for a fixed value of the pericenter height $h_{\text{peri}} = 4200 \text{ km}$. The dashed vertical line corresponds to $h_{\text{apo}} = 3.2 \times 10^6 \text{ km}$ which was the originally planned apocenter height of Juno before the problems encountered by its propulsion system.

Figures 1 to 2 deal with the pN gravitoelectric effects of Equations (58)–(63), while Figure 3 depicts the gravitomagnetic precessions of Equations (64)–(69). The conditions of Equations (53)–(54) and of Equation (73) were adopted in the calculation in order to obtain Figures 2 to 3.

According to Figure 1, the amplitude of the J_2/c^2 long-period signature of a ranges from $500 \text{ m yr}^{-1} = 0.01 \text{ mm s}^{-1}$ to $1100 \text{ m yr}^{-1} = 0.03 \text{ mm s}^{-1}$, a seemingly unexpected feature due to the impact of e in Equation (58) for increasingly larger values of it. Such figures are not far from the two-way Ka -band range rate residuals $\Delta\dot{\rho}$ of Juno displayed in [Iess et al. \(2018\)](#)

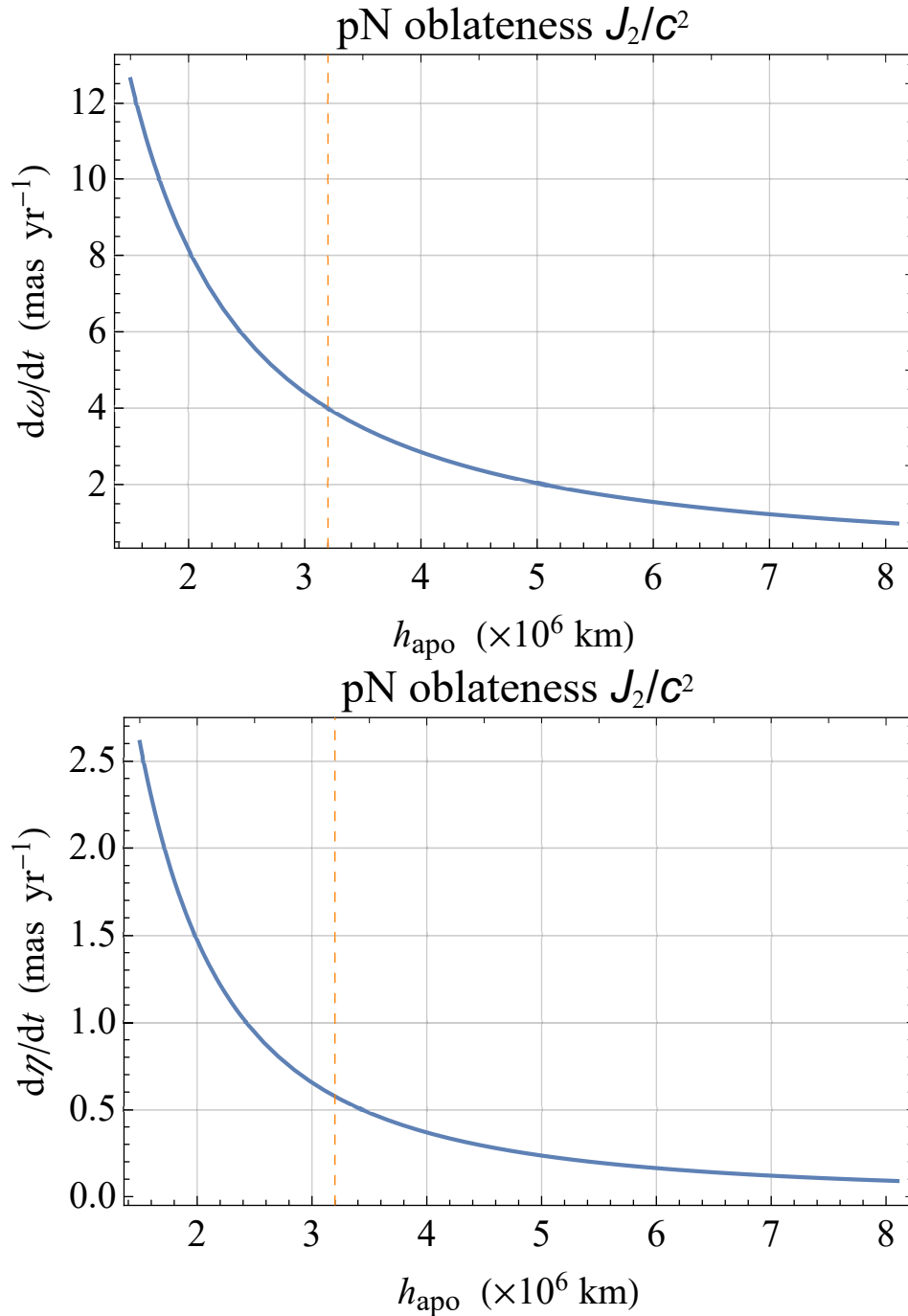


Figure 2. Plot of Equations (62)–(63), in mas yr^{-1} , calculated for the polar orbital configuration of Equations (53)–(54) with the condition of Equation (73), as functions of the apocenter height h_{apo} for a fixed value of the pericenter height $h_{\text{peri}} = 4200 \text{ km}$. The dashed vertical line corresponds to $h_{\text{apo}} = 3.2 \times 10^6 \text{ km}$ which was the originally planned apocenter height of Juno before the problems encountered by its propulsion system.

whose ranges of variation amount to 0.050 mm s^{-1} , with a root-mean-square value of 0.015 mm s^{-1} . However, caution is in order when such risky comparisons are made since the directly measurable range-rate and the theoretically computed semimajor axis are quite distinct quantities. As far as the J_2/c^2 effect on e is concerned, it turns out that, according to Table 1, the nominal value of Equation (70), which is a potentially major source of systematic bias, is smaller than it by about one order of magnitude. The J_2/c^2 pericentre precession, shown in Figure 2, is in the range $\approx 2 - 12$ milliarcseconds per year (mas yr^{-1}). It would be overwhelmed by the classical secular trend due to J_2 . Furthermore, both the latter and the 1pN signature are proportional to

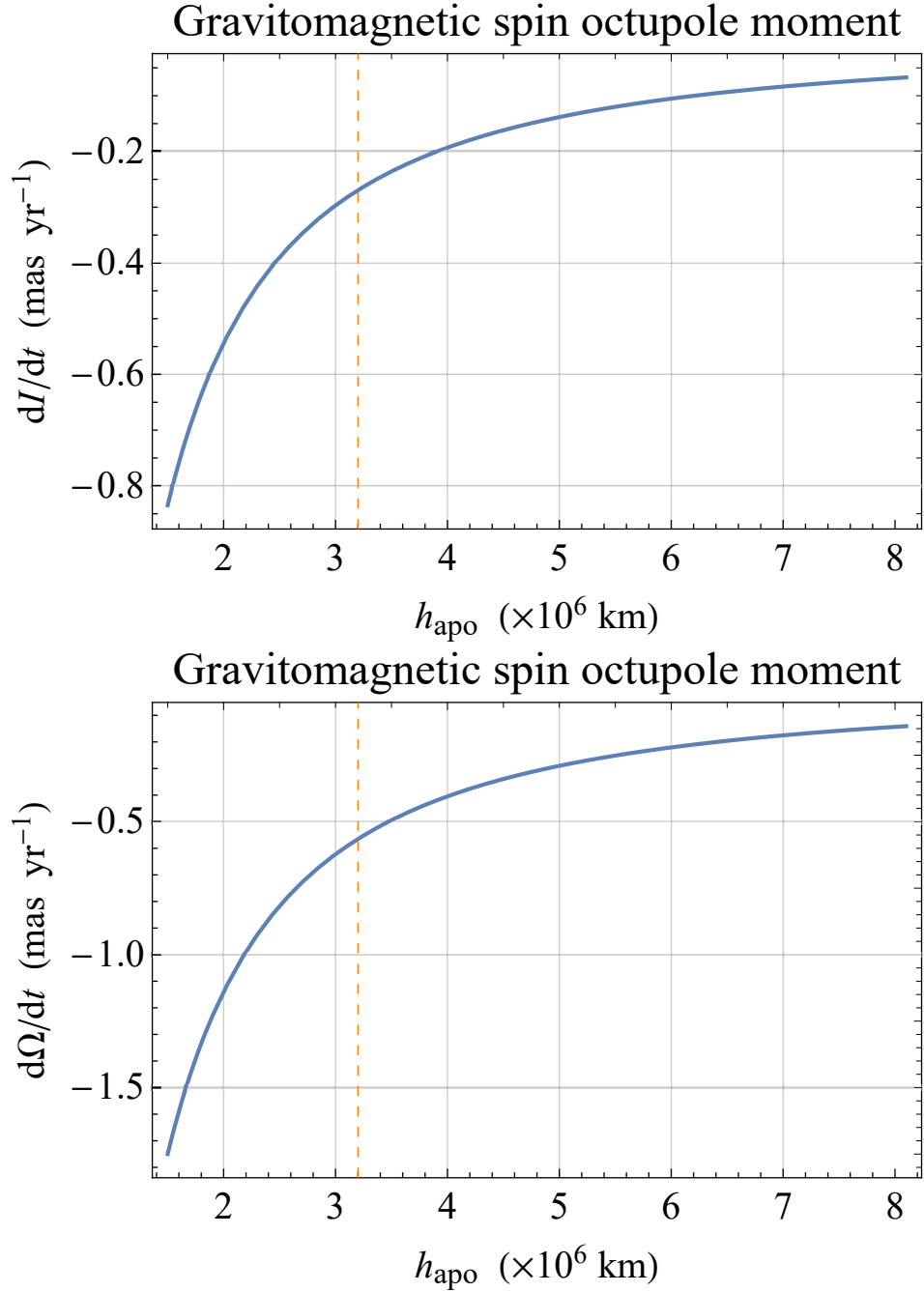


Figure 3. Plot of Equations (66)–(67), in mas yr^{-1} , calculated for the polar orbital configuration of Equations (53)–(54) with the condition of Equation (73), as functions of the apocenter height h_{apo} for a fixed value of the pericenter height $h_{\text{peri}} = 4200 \text{ km}$. The dashed vertical line corresponds to $h_{\text{apo}} = 3.2 \times 10^6 \text{ km}$ which was the originally planned apocenter height of Juno before the problems encountered by its propulsion system.

J_2 itself; their ratio is independent of it, so that one may not invoke any future improvement in our knowledge of the first even zonal of the Jovian gravity field to reduce the impact of the Newtonian effect on the 1pN one. A further potentially major source of systematic bias is represented by the competing classical N -body perturbations due to the Galilean moons of Jupiter, which orbit in its equatorial plane. It preliminarily turns out that⁹, if on the one hand, they leave the semimajor axis unaffected, on the other hand, for a polar orbit, they induce nonvanishing doubly-averaged orbital disturbances on e and ω . According to the

⁹ See Equations (1)–(5) of Iorio (2020) in which the parameters of the perturber are marked with \bullet .

present-day level of uncertainty¹⁰ in their masses as per the Planetary Satellite Ephemeris JUP365 (Jacobson 2021), the resulting mismodelled signatures of e and ω would be roughly one order of magnitude larger than, or about of the same order of magnitude of, the J_2/c^2 ones, apart for Callisto for which they are smaller than the pN ones. In the near future, the masses of the three outer Galilean satellites will be accurately determined by the JUperiter ICy moons Explorer (Grasset et al. 2013, JUICE;) and Clipper missions (Korth et al. 2022), while the flybys of Io by Juno should allow to improve the mass of Io as well. In particular, according to Tables 1–3 of Magnanini (2021), the masses of Europa, Ganymede, and Callisto should be determined by JUICE with an improvement of about 1–2 orders of magnitude with respect to the errors by Jacobson (2021).

Figure 3 tells us that the nonvanishing gravitomagnetic spin octupole orbital effects amount to $\approx 0.1 - 2 \text{ mas yr}^{-1}$. The impact of the Galilean moons of Jupiter would be of no concern for Equation (67) if viewed in a frame¹¹ aligned with the Jovian equator since the N -body node rate of change of a polar orbit acted upon by an equatorial perturber vanishes, as per Equation (4) of Iorio (2020). If, instead, the ICRF is adopted, the nonvanishing inclination of the orbits of the Galilean satellites to the Celestial Equator would make that the amplitudes of their mismodelled perturbations on I and Ω (Iorio 2020, Equations (4)-(5)) may be up to about one order of magnitude larger than Equations (66)–(67). The Sun does not represent an issue since it turns out that, by assuming $\sigma_{\mu_\odot} = 1 \times 10^{10} \text{ m}^3 \text{ s}^{-2}$ (Petit and Luzum 2010), its mismodelled classical perturbations are several orders of magnitude smaller than the pN effects of interest.

Despite inserting a spacecraft into a moderately elliptical orbits around Jupiter is a very daunting task because of the exceedingly amount of fuel required, we deem the study of the relativistic effects even in such an unlikely scenario worthy of investigation. By exploring the eccentricity range $e \approx 0.05 - 0.9$, with the pericenter height fixed to the value of Equation (74), yields the remarkable relativistic signatures of Figures 4 to 6.

¹⁰ See <https://ssd.jpl.nasa.gov/sats/phys-par/> on the Internet.

¹¹ In it, Equation (66) vanishes since $\delta = \pi/2$.

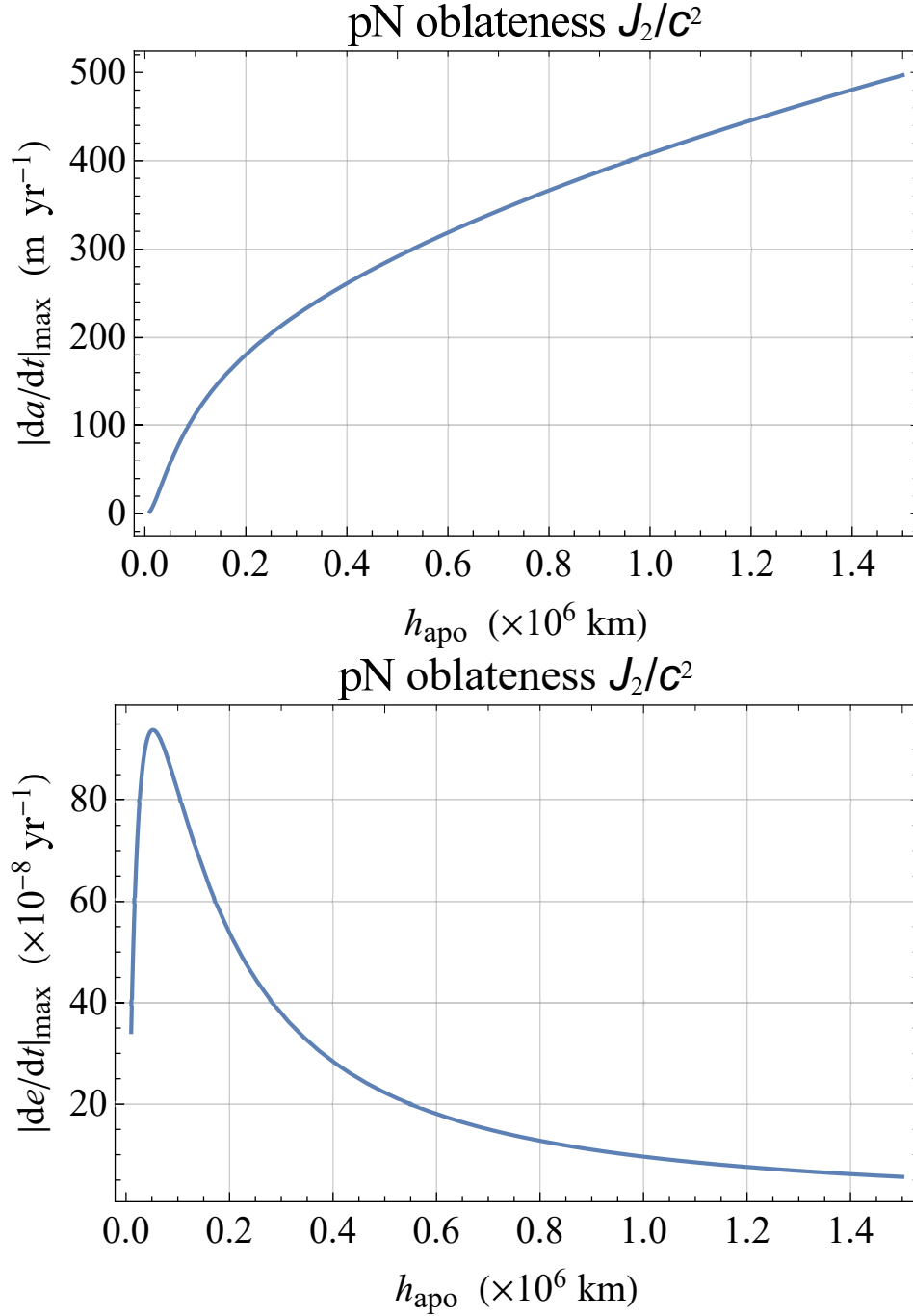


Figure 4. Plot of the amplitudes, in m yr^{-1} and 10^{-8} yr^{-1} , respectively, of Equations (58)–(59), calculated for the polar orbital configuration of Equations (53)–(54), as functions of the apocenter height h_{apo} for a fixed value of the pericenter height $h_{\text{peri}} = 4200 \text{ km}$.

In this case, the J_2/c^2 precessions can reach even the arcsec yr^{-1} level, while the gravitomagnetic signatures can be as large as a few hundred mas yr^{-1} . As far as the semimajor axis is concerned, the amplitude of its J_2/c^2 signature ranges from about $3 \text{ m yr}^{-1} = 3 \times 10^{-4} \text{ mm s}^{-1}$ to $500 \text{ m yr}^{-1} = 0.05 \text{ mm s}^{-1}$. Now, the mismodelled N -body orbital perturbations due to all the Galilean moons turn out to be negligible.

Such results demonstrate that, perhaps, it would be worth trying to actually carry out such a mission, however challenging it is. After all, it should not be neglected that, in addition to the relatively tiny pN effects induced by the multipoles of Jupiter, it could measure also the traditional and much larger pN mass monopole and spin-dipole effects.

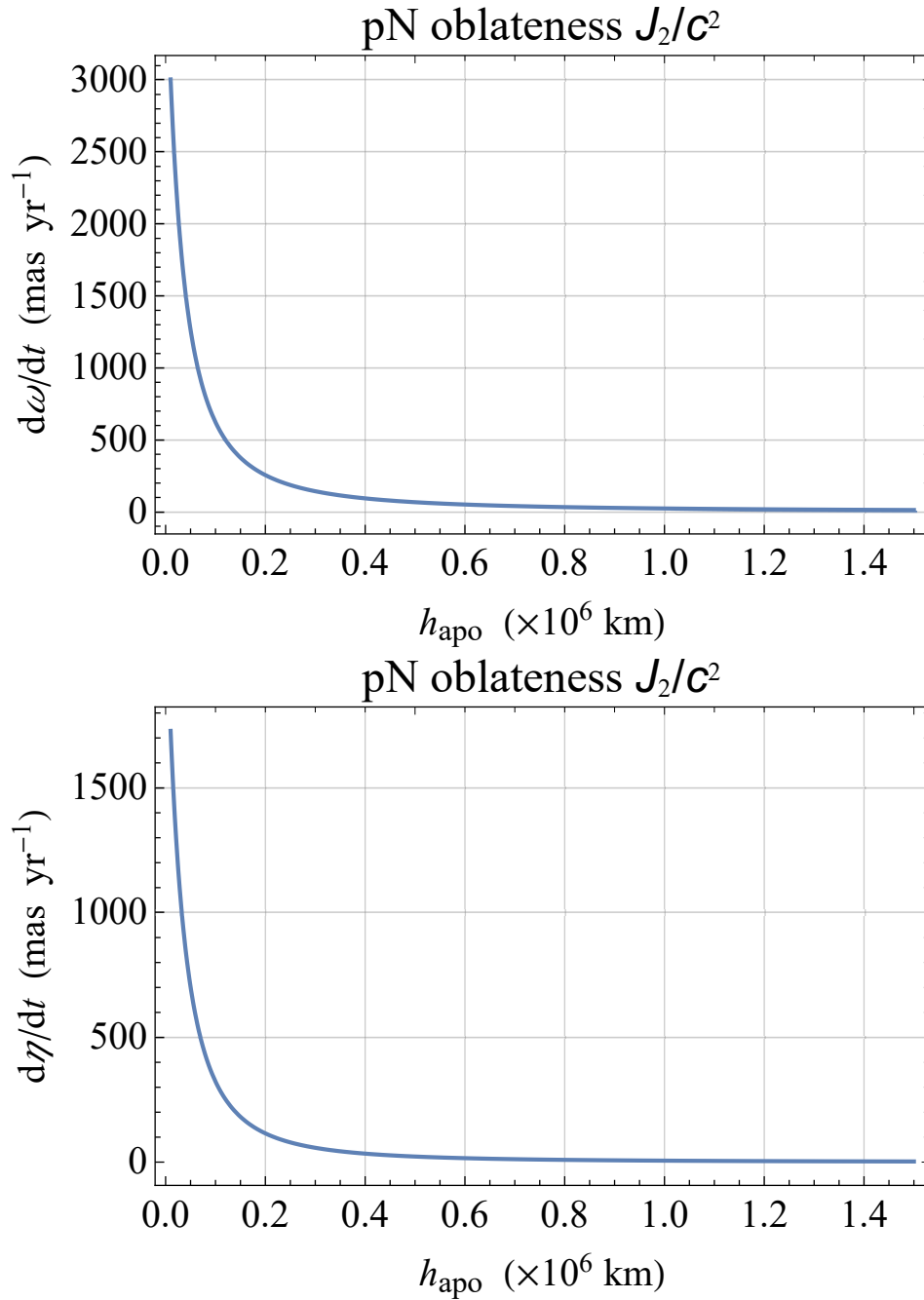


Figure 5. Plot of Equations (62)–(63), in mas yr^{-1} , calculated for the polar orbital configuration of Equations (53)–(54) with the condition of Equation (73), as functions of the apocenter height h_{apo} for a fixed value of the pericenter height $h_{\text{peri}} = 4200 \text{ km}$.

Incidentally, for, say, a Jovicentric Juno-like orbit, the aforementioned mixed effects of order $O(J_2^2/c^2)$ and $O(S \varepsilon^2 J_2/c^2)$ would be smaller than the direct ones retrievable in Figures 1 to 3 by a factor $\approx J_2 (R_e/a)^2 = 4 \times 10^{-6}$, as per Equation (76) and Table 1.

About the possibility of looking at Saturn as well, its relevant physical parameters are listed in Table 2. From them and from Table 1, it turns out that, despite the Kronian oblateness and ellipticity are slightly larger than the Jovian ones, the relativistic effects considered so far, with the same orbit, are larger for Jupiter by about one order of magnitude. Indeed, it is

$$\frac{M^{\text{Sat}} J_2^{\text{Sat}} (R_e^{\text{Sat}})^2}{M^{\text{Jup}} J_2^{\text{Jup}} (R_e^{\text{Jup}})^2} \approx 0.23, \quad (81)$$

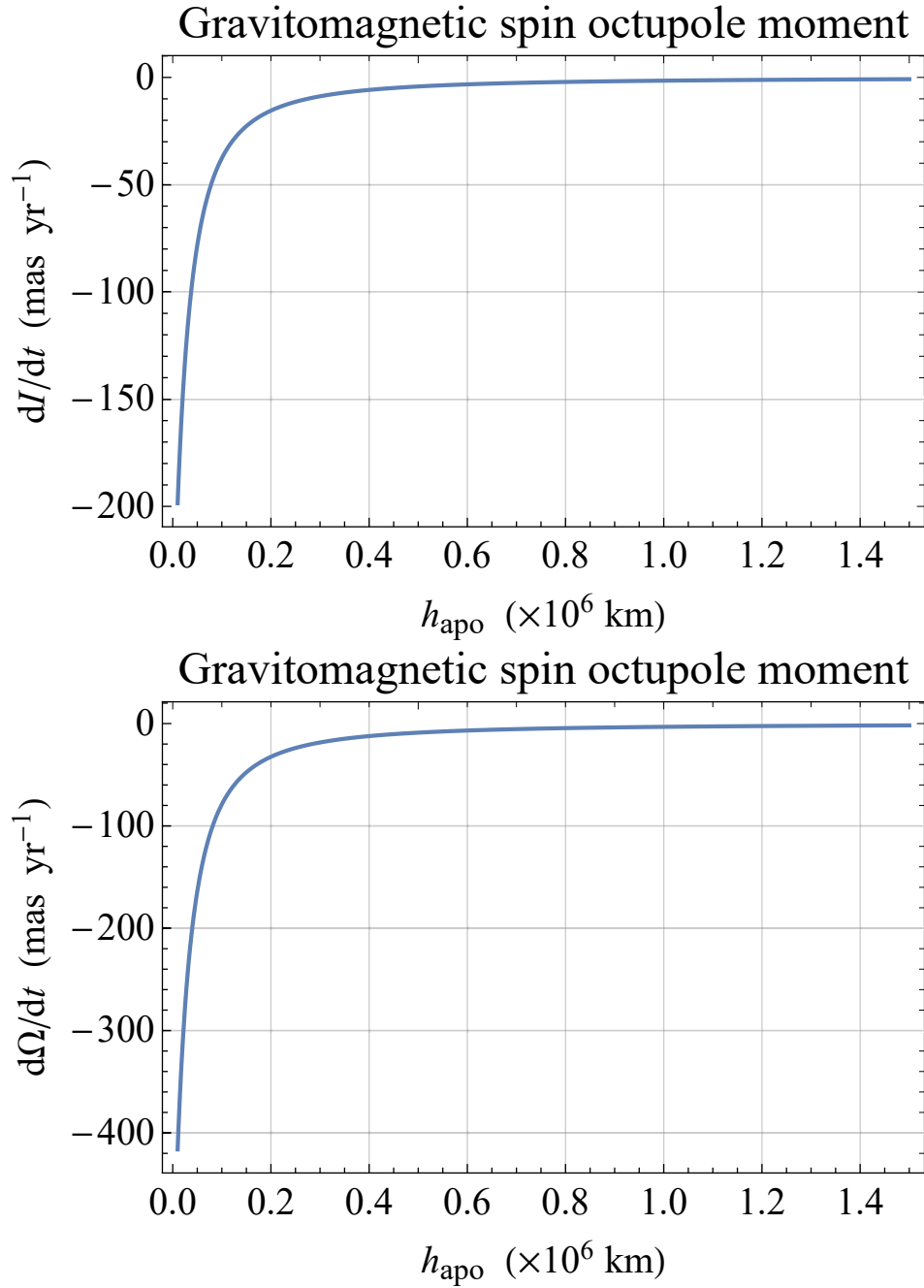


Figure 6. Plot of Equations (66)–(67), in mas yr^{-1} , calculated for the polar orbital configuration of Equations (53)–(54) with the condition of Equation (73), as functions of the apocenter height h_{apo} for a fixed value of the pericenter height $h_{\text{peri}} = 4200 \text{ km}$.

$$\frac{S_{\text{Sat}} (R_{\text{e}}^{\text{Sat}})^2 \varepsilon_{\text{Sat}}^2}{S_{\text{Jup}} (R_{\text{e}}^{\text{Jup}})^2 \varepsilon_{\text{Jup}}^2} \approx 0.21. \quad (82)$$

7. Probing the extended mass component in Sgr A *

Table 2. Relevant physical parameters of Saturn (Soffel et al. 2003; Seidelmann et al. 2007; Jacobson 2022). The value for the ellipticity ε is obtained from the figures reported for R_e and R_p .

Parameter	Units	Numerical value
μ	$\text{m}^3 \text{s}^{-2}$	3.79312×10^{16} (Jacobson 2022)
J_2	$\times 10^{-6}$	16290.615 (Jacobson 2022)
S	$\text{kg m}^2 \text{s}^{-1}$	1.4×10^{38} (Soffel et al. 2003)
α	deg	40.594872 (Jacobson 2022)
δ	deg	83.534351 (Jacobson 2022)
R_e	km	60268 (Seidelmann et al. 2007)
R_p	km	54364 (Seidelmann et al. 2007)
ε	–	0.431

The general validity of Equations (15)–(20) and of Equations (25)–(30) allows one to apply them, in principle, also to the highly elliptical paths of the S stars (Ali et al. 2020) orbiting the supermassive black hole (SMBH) in Sgr A* at the Galactic Center (Ghez et al. 2008; Genzel et al. 2010) in order, e.g., to characterize the predicted mass component enclosed by the stellar orbits¹² (Gondolo and Silk 1999; Mouawad et al. 2005; Gillessen et al. 2009; Chan et al. 2022). Such an extended dark mass distribution surrounding Sgr A* might be made of faint S stars, neutron stars, stellar mass black holes, faint accretion gas clouds, stellar remnants and nonbaryonic dark matter as well. Should it has departures from spherical symmetry, they may be dynamically probed, in principle, with the pN orbital effects investigated here.

As far as the SMBH itself is concerned, its direct effects are too small to be of any relevance. As an example, with the replacement

$$J_2 \rightarrow -\frac{Q_2}{M R_e^2} \quad (83)$$

in Equation (15), by using¹³ (Carter 1971; Robinson 1975)

$$Q_2^* = -\frac{S_\bullet^2}{c^2 M_\bullet} \quad (84)$$

and (Kerr 1963; Teukolsky 2015)

$$S_\bullet = \chi_g \frac{M_\bullet^2 G}{c}, \quad (85)$$

the amplitude of Equation (15) can be cast into the form

$$\frac{da}{dt} \propto -\frac{9 e^2 (6 + e^2) \pi^3 \chi_g^2 \mu_\bullet^2}{c^6 (1 - e^2)^4 P_b^3}. \quad (86)$$

In the case of the recently discovered star S4716, characterized by $P_b = 4.02 \text{ yr}$, $e = 0.756$ (Peißker et al. 2022), Equation (86) yields¹⁴

$$\left| \frac{da}{dt} \right| \propto 7 \times 10^{-11} \text{ m yr}^{-1}. \quad (87)$$

8. Summary and conclusions

We analytically worked out the pN orbital effects induced on a test particle by the quadrupole mass moment and the gravitomagnetic spin octupole moment of an axisymmetric rotating body. The resulting explicit expressions of the long-term rates of change of the satellite’s osculating Keplerian orbital elements, averaged over one orbital period, retain a general validity since they hold for any orbital configuration and for an arbitrary orientation of the body’s spin axis in space. In general, they are all nonzero, with the exception of the gravitomagnetic variation of the semimajor axis which vanishes over an orbital revolution.

¹² Until now, only the S2 star has been used to this aim; see, e.g., Rubilar and Eckart (2001); Nucita et al. (2007); Zakharov et al. (2007); Dokuchaev and Eroshenko (2015b,a); Heißel et al. (2022); Argüelles et al. (2022); GRAVITY Collaboration et al. (2022).

¹³ It is a manifestation of the celebrated “no-hair theorem” (Carter 1971; Robinson 1975) according to which the mass M_\bullet^l and the spin S_\bullet^l moments of a Kerr black hole (Geroch 1970; Hansen 1974) are connected by the relation $M_\bullet^l + i S_\bullet^l = M_\bullet (i S_\bullet / c M_\bullet)^l$, where $i = \sqrt{-1}$. The odd mass moments and even spin moments are identically zero; M_\bullet^2 is the quadrupole mass moment, corresponding just to Equation (84).

¹⁴ The values $\chi_g = 0.5$, $M_\bullet = 4.1 \times 10^6 M_\odot$ (Peißker et al. 2020, 2022) were used in Equation (86).

Our results were subsequently specialized to two particular orbital geometries: (a) an equatorial orbit; (b) a polar orbit. In the scenario a), only the pericenter and the mean anomaly at epoch undergo nonzero net effects for both the pN accelerations considered; such orbital features of motion turn out to be genuine secular trends. The scenario b) is more complex. Indeed, in the case of the pN oblateness, only the inclination and the node stay constant. While the semimajor axis and the eccentricity experience purely long-period variations because of the generally varying pericenter entering the expressions of their averaged rates of change, the pericenter and the mean anomaly at epoch are affected also by secular trends in addition to long-period signals. It should be recalled that, in a realistic scenario, the pericenter does change mainly because of the zonal harmonics of the Newtonian part of the multipolar expansion of the gravitational potential of the central body. As far as the gravitomagnetic octupolar field is concerned, the only orbital elements that vary, on average, are the inclination and the node; they experience both secular and long-period effects.

The case b) was applied to a hypothetical scenario around Jupiter by first adopting the same pericenter height of the current Juno spacecraft and varying the apocenter height in such a way that the eccentricity ranged from $e = 0.92$ to the Juno's present value $e = 0.98$. The resulting amplitude of the long-period pN signature of the semimajor axis due to the Jovian oblateness is comprised within $500 \text{ m yr}^{-1} = 0.01 \text{ mm s}^{-1}$ ($e = 0.92$) and $1100 \text{ m yr}^{-1} = 0.03 \text{ mm s}^{-1}$ ($e = 0.98$). Although the following improper comparison is potentially misleading, it may be interesting to cautiously noting that the present-day accuracy level in measuring the range-rate shift of Juno is just at the $\approx 0.01 \text{ mm s}^{-1}$ level. The other nonvanishing pN oblateness-driven effects on the pericenter and the mean anomaly at epoch amount to about $2 - 12 \text{ mas yr}^{-1}$, while the gravitomagnetic rates of the inclination and the node are at the $\approx 0.1 - 2 \text{ mas yr}^{-1}$ level. Then, much less elliptical orbits with the same pericenter of Juno were considered, although they are at present almost impossible to achieve practically. In this case, the pN gravitoelectric rates can be as large as $\approx 1 - 3 \text{ arcsec yr}^{-1}$, while the spin octupole effects can reach the level of a few hundred mas yr^{-1} . Given the same orbital configuration, it turns out that the aforementioned effects around Saturn would be about an order of magnitude smaller.

Another potentially viable scenario for our results is represented by the highly elliptical orbits of the S stars moving around the supermassive black hole in Sgr A* at the Galactic Center. Indeed, it is likely surrounded by an extended matter distribution which can be made either of nonbaryonic dark matter or by the remnants of tidally disrupted stars, pulsars, etc. Such a halo is not necessarily spherically symmetric, and, in principle, the orbital effects calculated here may be useful to get more information on it.

A. Notations and definitions

Here, some basic notations and definitions used throughout the text are presented (Soffel 1989; Brumberg 1991; Bertotti et al. 2003; Kopeikin et al. 2011; Poisson and Will 2014; Soffel and Han 2019).

G : Newtonian constant of gravitation

c : speed of light in vacuum

M : mass of the central body

M_{\odot} : mass of the Sun

$\mu := GM$: gravitational parameter of the central body

\mathbf{S} : angular momentum of the central body

S : magnitude of the angular momentum of central body

χ_g : dimensionless spin parameter of a Kerr black hole: it is $|\chi_g| \leq 1$.

$\hat{\mathbf{k}} = \{\hat{k}_x, \hat{k}_y, \hat{k}_z\}$: spin axis of the central body with respect to some reference frame

α : longitude of the spin axis of the central body in some reference frame

δ : latitude of the spin axis of the central body in some reference frame

$\hat{k}_x = \cos \alpha \cos \delta$: x component of the spin axis of the central body with respect to some reference frame

$\hat{k}_y = \sin \alpha \cos \delta$: y component of the spin axis of the central body with respect to some reference frame

$\hat{k}_z = \sin \delta$: z component of the spin axis of the central body with respect to some reference frame

R_e : equatorial radius of the central body

R_p : polar radius of the central body

$\varepsilon := \sqrt{1 - \left(\frac{R_p}{R_e}\right)^2}$: ellipticity of the central body

J_2 : dimensionless zonal harmonic coefficient of degree $\ell = 2$ of the non spherically symmetric gravitational potential of the central body

Q_2 : dimensional mass quadrupole moment of the non spherically symmetric gravitational potential of the central body

\mathbf{B}^{oct} : gravitomagnetic spin octupole field in the empty space surrounding the rotating central body

ϕ^{oct} : gravitomagnetic spin octupole potential in the empty space surrounding the rotating central body

\mathbf{A} : perturbing acceleration experienced by the test particle

\mathbf{r} : position vector of the test particle with respect to the central body

r : distance of the test particle from the central body

$\hat{\mathbf{r}} := \mathbf{r}/r$: radial unit vector

$\xi := \hat{\mathbf{k}} \cdot \hat{\mathbf{r}}$: cosine of the angle between the central body's spin axis and the position vector of the test particle

\mathbf{v} : velocity vector of the test particle

$v_r := \mathbf{v} \cdot \hat{\mathbf{r}}$: radial velocity of the test particle

$\lambda := \hat{\mathbf{k}} \cdot \mathbf{v}$: projection of the velocity of the test particle onto the direction of the spin axis of the central body

$\mathcal{P}_\ell(\dots)$: Legendre polynomial of degree ℓ

a : semimajor axis of the test particle

$n_b := \sqrt{\mu/a^3}$: Keplerian mean motion of the test particle

$P_b := 2\pi/n_b$: orbital period of the test particle

e : eccentricity of the test particle

$p := a(1 - e^2)$: semilatus rectum of the orbit of the test particle

I : inclination of the orbital plane of the test particle to the plane $\{x, y\}$ of some reference frame

Ω : longitude of the ascending node of the test particle

ω : argument of pericenter of the test particle

η : mean anomaly at epoch

f : true anomaly of the test particle

$u := \omega + f$: argument of latitude of the test particle

$\hat{\mathbf{I}} := \{\cos \Omega, \sin \Omega, 0\}$: unit vector directed along the line of the nodes toward the ascending node

$\hat{\mathbf{m}} := \{-\cos I \sin \Omega, \cos I \cos \Omega, \sin I\}$: unit vector directed transversely to the line of the nodes in the orbital plane

$\hat{\mathbf{h}} := \{\sin I \sin \Omega, -\sin I \cos \Omega, \cos I\}$: normal unit vector such that $\hat{\mathbf{I}} \times \hat{\mathbf{m}} = \hat{\mathbf{h}}$

$\hat{\mathbf{t}} = \hat{\mathbf{h}} \times \hat{\mathbf{r}}$: transverse unit vector

$A_R := \mathbf{A} \cdot \hat{\mathbf{r}}$: radial component of the perturbing acceleration \mathbf{A}

$A_T := \mathbf{A} \cdot \hat{\mathbf{t}}$: transverse component of the perturbing acceleration \mathbf{A}

$A_N := \mathbf{A} \cdot \hat{\mathbf{h}}$: normal component of the perturbing acceleration \mathbf{A}

B. Coefficients \widehat{T}_j of the orbital rates of changes

The coefficients \widehat{T}_j , $j = 1, 2, \dots, 6$ entering Equations (15)–(20) in Section 3 and Equations (25)–(30) in Section 4 are

$$\widehat{T}_1 := 1, \quad (\text{B1})$$

$$\widehat{T}_2 := \left[(\hat{\mathbf{k}} \cdot \hat{\mathbf{l}})^2 + (\hat{\mathbf{k}} \cdot \hat{\mathbf{m}})^2 \right], \quad (\text{B2})$$

$$\widehat{T}_3 := \left[(\hat{\mathbf{k}} \cdot \hat{\mathbf{l}})^2 - (\hat{\mathbf{k}} \cdot \hat{\mathbf{m}})^2 \right], \quad (\text{B3})$$

$$\widehat{T}_4 := \left[(\hat{\mathbf{k}} \cdot \hat{\mathbf{h}}) (\hat{\mathbf{k}} \cdot \hat{\mathbf{l}}) \right], \quad (\text{B4})$$

$$\widehat{T}_5 := \left[(\hat{\mathbf{k}} \cdot \hat{\mathbf{h}}) (\hat{\mathbf{k}} \cdot \hat{\mathbf{m}}) \right], \quad (\text{B5})$$

$$\widehat{T}_6 := \left[(\hat{\mathbf{k}} \cdot \hat{\mathbf{l}}) (\hat{\mathbf{k}} \cdot \hat{\mathbf{m}}) \right]. \quad (\text{B6})$$

References

- B. Ali, D. Paul, A. Eckart, M. Parsa, M. Zajacek, F. Peißker, M. Subroweit, M. Valencia-S., L. Thomkins, and G. Witzel. Kinematic Structure of the Galactic Center S Cluster. *Astrophys. J.*, 896(2):100, Jun 2020. <https://doi.org/10.3847/1538-4357/ab93ae>.
- J. D. Anderson, M. S. W. Keeseey, E. L. Lau, E. M. Standish, Jr., and X. X. Newhall. Tests of general relativity using astrometric and radio metric observations of the planets. *Acta Astronaut.*, 5:43–61, Feb 1978. [https://doi.org/10.1016/0094-5765\(78\)90034-6](https://doi.org/10.1016/0094-5765(78)90034-6).
- J. D. Anderson, J. K. Campbell, R. F. Jurgens, E. L. Lau, X. Newhall, X. A. Slade III, M. and M. Standish Jr, E. Recent developments in solar-system tests of general relativity. In F. Satō and T. Nakamura, editors, *Proceedings of the Sixth Marcel Grossmann Meeting on General Relativity*, pages 353–355. World Scientific, Singapore, Jan 1993.
- C. R. Argüelles, M. F. Mestre, E. A. Becerra-Vergara, V. Crespi, A. Krut, J. A. Rueda, and R. Ruffini. What does lie at the Milky Way centre? Insights from the S2-star orbit precession. *Mon. Not. Roy. Astron. Soc.*, 511(1):L35–L39, Mar 2022. <https://doi.org/10.1093/mnrasl/slab126>.
- B. Bertotti, P. Farinella, and D. Vokrouhlický. *Physics of the Solar System*. Kluwer, Dordrecht, Aug 2003. <https://doi.org/10.1007/978-94-010-0233-2>.
- S. J. Bolton, J. Lunine, D. Stevenson, J. E. P. Connerney, S. Levin, T. C. Owen, F. Bagenal, D. Gautier, A. P. Ingersoll, G. S. Orton, T. Guillot, W. Hubbard, J. Bloxham, A. Coradini, S. K. Stephens, P. Mokashi, R. Thorne, and R. Thorpe. The Juno Mission. *Space Sci. Rev.*, 213(1-4):5–37, Nov 2017. <https://doi.org/10.1007/s11214-017-0429-6>.
- V. A. Brumberg. *Essential Relativistic Celestial Mechanics*. Adam Hilger, Bristol, 1991.
- M. Capderou. *Satellites. Orbits and Missions*. Springer-Verlag France, Paris, Mar 2005. <https://doi.org/10.1007/b139118>.
- B. Carter. Axisymmetric Black Hole Has Only Two Degrees of Freedom. *Phys. Rev. Lett.*, 26(6):331–333, Feb 1971. <https://doi.org/10.1103/PhysRevLett.26.331>.
- M. H. Chan, C. M. Lee, and C. W. Yu. Investigating the nature of mass distribution surrounding the Galactic supermassive black hole. *Sci. Rep.*, 12:15258, Sep 2022. <https://doi.org/10.1038/s41598-022-18946-7>.
- V. I. Dokuchaev and Y. N. Eroshenko. Weighing of the dark matter at the center of the galaxy. *J. Exp. Theor. Phys.*, 101(12):777–782, Jun 2015a. <https://doi.org/10.1134/S0021364015120048>.
- V. I. Dokuchaev and Y. N. Eroshenko. Physical laboratory at the center of the Galaxy. *Phys.-Uspekhi*, 58(8):772–784, Aug 2015b. <https://doi.org/10.3367/UFNe.0185.201508c.0829>.
- A. Einstein. Erklärung der Perihelbewegung des Merkur aus der allgemeinen Relativitätstheorie. *Sitzber. Preuss. Akad.*, 47:831–839, Nov 1915.
- C. W. F. Everitt. The Gyroscope experiment - I: General description and analysis of gyroscope performance. In B. Bertotti, editor, *Proceedings of the International School of Physics “Enrico Fermi”*. Course LVI. *Experimental Gravitation*, pages 331–360. Academic Press, New York and London, 1974.
- C. W. F. Everitt, S. Buchman, D. B. Debra, G. M. Keiser, J. M. Lockhart, B. Muhlfelder, B. W. Parkinson, and J. P. Turneaure. Gravity Probe B: Countdown to Launch. In C. Lämmerzahl, C. W. F. Everitt, and F. W. Hehl, editors, *Gyros, Clocks, Interferometers ...: Testing Relativistic Gravity in Space*, volume 562 of *Lecture Notes in Physics*, pages 52–82. Springer Verlag, Berlin, Feb 2001. https://doi.org/10.1007/3-540-40988-2_4.
- C. W. F. Everitt, D. B. Debra, B. W. Parkinson, J. P. Turneaure, J. W. Conklin, M. I. Heifetz, G. M. Keiser, A. S. Silbergleit, T. Holmes, J. Kolodziejczak, M. Al-Meshari, J. C. Mester, B. Muhlfelder, V. G. Solomonik, K. Stahl, P. W. Worden, Jr., W. Bencze, S. Buchman, B. Clarke, A. Al-Jadaan, H. Al-Jibreen, J. Li, J. A. Lipa, J. M. Lockhart, B. Al-Suwaidan, M. Taber, and S. Wang. Gravity Probe B: Final Results of a Space Experiment to Test General Relativity. *Phys. Rev. Lett.*, 106(22):221101, Jun 2011. <https://doi.org/10.1103/PhysRevLett.106.221101>.

- C. W. F. Everitt, B. Muhlfelder, D. B. DeBra, B. W. Parkinson, J. P. Turneure, A. S. Silbergleit, E. B. Acworth, M. Adams, R. Adler, W. J. Benzec, J. E. Berberian, R. J. Bernier, K. A. Bower, R. W. Brumley, S. Buchman, K. Burns, B. Clarke, J. W. Conklin, M. L. Eglington, G. Green, G. Gutt, D. H. Gwo, G. Hanuschak, X. He, M. I. Heifetz, D. N. Hipkins, T. J. Holmes, R. A. Kahn, G. M. Keiser, J. A. Kozaczuk, T. Langenstein, J. Li, J. A. Lipa, J. M. Lockhart, M. Luo, I. Mandel, F. Marcelja, J. C. Mester, A. Ndili, Y. Ohshima, J. Overduin, M. Salomon, D. I. Santiago, P. Shestople, V. G. Solomonik, K. Stahl, M. Taber, R. A. Van Patten, S. Wang, J. R. Wade, P. W. Worden, Jr., N. Bartel, L. Herman, D. E. Lebach, M. Ratner, R. R. Ransom, I. I. Shapiro, H. Small, B. Strozozas, R. Geveden, J. H. Goebel, J. Horack, J. Kolodziejczak, A. J. Lyons, J. Olivier, P. Peters, M. Smith, W. Till, L. Wooten, W. Reeve, M. Anderson, N. R. Bennett, K. Burns, H. Dougherty, P. Dulgov, D. Frank, L. W. Huff, R. Katz, J. Kirschenbaum, G. Mason, D. Murray, R. Parmley, M. I. Ratner, G. Reynolds, P. Rittmuller, P. F. Schweiger, S. Shehata, K. Triebes, J. VandenBeukel, R. Vassar, T. Al-Saud, A. Al-Jadaan, H. Al-Jibreen, M. Al-Meshari, and B. Al-Suwaidan. The Gravity Probe B test of general relativity. *Class. Quantum Gravit.*, 32(22):224001, Nov 2015. <https://doi.org/10.1088/0264-9381/32/22/224001>.
- F. Frutos-Alfaro and M. H. Soffel. On relativistic multipole moments of stationary space-times. *R. Soc. Open Sci.*, 5(7):180640, Jul 2018. <https://doi.org/10.1098/rsos.180640>.
- R. Genzel, F. Eisenhauer, and S. Gillessen. The Galactic Center massive black hole and nuclear star cluster. *Rev. Mod. Phys.*, 82(4):3121–3195, Oct 2010. <https://doi.org/10.1103/RevModPhys.82.3121>.
- R. Geroch. Multipole Moments. II. Curved Space. *J. Math. Phys.*, 11(8):2580–2588, Aug 1970. <https://doi.org/10.1063/1.1665427>.
- A. M. Ghez, S. Salim, N. N. Weinberg, J. R. Lu, T. Do, J. K. Dunn, K. Matthews, M. R. Morris, S. Yelda, E. E. Becklin, T. Kremenek, M. Milosavljevic, and J. Naiman. Measuring Distance and Properties of the Milky Way’s Central Supermassive Black Hole with Stellar Orbits. *Astrophys. J.*, 689(2):1044–1062, Dec 2008. <https://doi.org/10.1086/592738>.
- S. Gillessen, F. Eisenhauer, S. Trippe, T. Alexander, R. Genzel, F. Martins, and T. Ott. Monitoring Stellar Orbits Around the Massive Black Hole in the Galactic Center. *Astrophys. J.*, 692(2):1075–1109, Feb 2009. <https://doi.org/10.1088/0004-637X/692/2/1075>.
- P. Gondolo and J. Silk. Dark Matter Annihilation at the Galactic Center. *Phys. Rev. Lett.*, 83(9):1719–1722, Aug 1999. <https://doi.org/10.1103/PhysRevLett.83.1719>.
- O. Grasset, M. K. Dougherty, A. Coustenis, E. J. Bunce, C. Erd, D. Titov, M. Blanc, A. Coates, P. Drossart, L. N. Fletcher, H. Hussmann, R. Jaumann, N. Krupp, J.-P. Lebreton, O. Prieto-Ballesteros, P. Tortora, F. Tosi, and T. Van Hoolst. Jupiter ICy moons Explorer (JUICE): An ESA mission to orbit Ganymede and to characterise the Jupiter system. *Planet. Space Sci.*, 78:1–21, Apr 2013. <https://doi.org/10.1016/j.pss.2012.12.002>.
- GRAVITY Collaboration, R. Abuter, A. Amorim, M. Bauböck, J. P. Berger, H. Bonnet, W. Brandner, V. Cardoso, Y. Clénet, P. T. de Zeeuw, J. Dexter, A. Eckart, F. Eisenhauer, N. M. Förster Schreiber, P. Garcia, F. Gao, E. Gendron, R. Genzel, S. Gillessen, M. Habibi, X. Hauboiss, T. Henning, S. Hippler, M. Horrobin, A. Jiménez-Rosales, L. Jochum, L. Jocou, A. Kaufer, P. Kervella, S. Lacour, V. Lapeyrière, J. B. Le Bouquin, P. Léna, M. Nowak, T. Ott, T. Paumard, K. Perraut, G. Perrin, O. Pfuhl, G. Rodríguez-Coira, J. Shangguan, S. Scheithauer, S. Scheithauer, J. Stadler, O. Straub, C. Straubmeier, E. Sturm, L. J. Tacconi, F. Vincent, S. von Fellenberg, I. Waisberg, F. Widmann, E. Wieprecht, E. Wiezorrek, J. Woillez, S. Yazici, and G. Zins. Detection of the Schwarzschild precession in the orbit of the star S2 near the Galactic centre massive black hole. *Astron. Astrophys.*, 636:L5, Apr 2020. <https://doi.org/10.1051/0004-6361/202037813>.
- GRAVITY Collaboration, R. Abuter, A. Aimar, N. Amorim, J. Ball, M. Bauböck, J. P. Berger, H. Bonnet, G. Bourdarot, W. Brandner, V. Cardoso, Y. Clénet, Y. Dallilar, R. Davies, P. T. de Zeeuw, J. Dexter, A. Drescher, F. Eisenhauer, N. M. Förster Schreiber, A. Foschi, P. Garcia, F. Gao, E. Gendron, R. Genzel, S. Gillessen, M. Habibi, X. Hauboiss, G. Heiße, T. Henning, S. Hippler, M. Horrobin, L. Jochum, L. Jocou, A. Kaufer, P. Kervella, S. Lacour, V. Lapeyrière, J. B. Le Bouquin, P. Léna, D. Lutz, T. Ott, T. Paumard, K. Perraut, G. Perrin, O. Pfuhl, S. Rabien, J. Shangguan, T. Shimizu, S. Scheithauer, J. Stadler, A. W. Stephens, O. Straub, C. Straubmeier, E. Sturm, L. J. Tacconi, K. R. W. Tristram, F. Vincent, S. von Fellenberg, F. Widmann, E. Wieprecht, E. Wiezorrek, J. Woillez, S. Yazici, and A. Young. Mass distribution in the Galactic Center based on interferometric astrometry of multiple stellar orbits. *Astron. Astrophys.*, 657:L12, Jan 2022. <https://doi.org/10.1051/0004-6361/202142465>.
- M. R. Haas and D. K. Ross. Measurement of the Angular Momentum of Jupiter and the Sun by Use of the Lense-Thirring Effect. *Astrophys. Space Sci.*, 32(1):3–11, Jan 1975. <https://doi.org/10.1007/BF00646213>.
- R. O. Hansen. Multipole moments of stationary space-times. *J. Math. Phys.*, 15(1):46–52, Jan 1974. <https://doi.org/10.1063/1.1666501>.
- J. Heimberger, M. Soffel, and H. Ruder. Relativistic effects in the motion of artificial satellites - The oblateness of the central body II. *Celest. Mech. Dyn. Astr.*, 47(2):205–217, Jun 1989. <https://doi.org/10.1007/BF00051205>.
- G. Heiße, T. Paumard, G. Perrin, and F. Vincent. The dark mass signature in the orbit of S2. *Astron. Astrophys.*, 660:A13, Apr 2022. <https://doi.org/10.1051/0004-6361/202142114>.
- C. Huang and L. Liu. Analytical solutions to the four post-Newtonian effects in a near Earth satellite orbit. *Celest. Mech. Dyn. Astr.*, 53(3):293–307, Sep 1992. <https://doi.org/10.1007/BF00052615>.
- L. Iess, W. M. Folkner, D. Durante, M. Parisi, Y. Kaspi, E. Galanti, T. Guillot, W. B. Hubbard, D. J. Stevenson, J. D. Anderson, D. R. Buccino, L. G. Casajus, A. Milani, R. Park, P. Racioppa, D. Serra, P. Tortora, M. Zannoni, H. Cao, R. Helled, J. I. Lunine, Y. Miguel, B. Militzer, S. Wahl, J. E. P. Connerney, S. M. Levin, and S. J. Bolton. Measurement of Jupiter’s asymmetric gravity field. *Nature*, 555(7695):220–222, Mar 2018. <https://doi.org/10.1038/nature25776>.
- L. Iorio. Juno, the angular momentum of Jupiter and the Lense-Thirring effect. *New Astron.*, 15(6):554–560, Aug 2010. <https://doi.org/10.1016/j.newast.2010.01.004>.
- L. Iorio. Post-Newtonian direct and mixed orbital effects due to the oblateness of the central body. *Int. J. Mod. Phys. D*, 24(8):1550067–59, Jun 2015. <https://doi.org/10.1142/S0218271815500674>.
- L. Iorio. The post-Newtonian gravitomagnetic spin-Octupole moment of an oblate rotating body and its effects on an orbiting test particle; are they measurable in the Solar system? *Mon. Not. Roy. Astron. Soc.*, 484(4):4811–4832, Apr 2019a. <https://doi.org/10.1093/mnras/stz304>.
- L. Iorio. Erratum: The post-Newtonian gravitomagnetic spin-octupole moment of an oblate rotating body and its effects on an orbiting test particle; are they measurable in the Solar system? *Mon. Not. Roy. Astron. Soc.*, 485(3):4090–4090, May 2019b. <https://doi.org/10.1093/mnras/stz699>.
- L. Iorio. A HERO for General Relativity. *Universe*, 5(7):165, Jul 2019c. <https://doi.org/10.3390/universe5070165>.
- L. Iorio. What Would Happen if We Were About 1 pc Away from a Supermassive Black Hole? *Astrophys. J.*, 889(2):152, Feb 2020. <https://doi.org/10.3847/1538-4357/ab5d2a>.
- L. Iorio. The post-Newtonian motion around an oblate spheroid: the mixed orbital effects due to the Newtonian oblateness and the post-Newtonian mass monopole accelerations. *arXiv e-prints*, art. arXiv:2310.02838, Oct 2023. <https://doi.org/10.48550/arXiv.2310.02838>. at press in *Gen. Relativ. Gravit.*
- L. Iorio, H. I. M. Lichtenegger, M. L. Ruggiero, and C. Corda. Phenomenology of the Lense-Thirring effect in the solar system. *Astrophys. Space Sci.*, 331(2):351–395, Feb 2011. <https://doi.org/10.1007/s10509-010-0489-5>.
- L. Iorio, A. P. Girija, and D. Durante. One EURO for Uranus: the Elliptical Uranian Relativity Orbiter mission. *Mon. Not. Roy. Astron. Soc.*, 523(3):3595–3614, Aug 2023. <https://doi.org/10.1093/mnras/stad1446>.
- R. A. Jacobson. The Orbits of the Regular Jovian Satellites and the Orientation of the Pole of Jupiter. Personal communication to Horizons/NAIF, 2021.
- R. A. Jacobson. The Orbits of the Main Saturnian Satellites, the Saturnian System Gravity Field, and the Orientation of Saturn’s Pole. *Astron. J.*, 164(5):199, Nov 2022. <https://doi.org/10.3847/1538-3881/ac90c9>.

- R. P. Kerr. Gravitational Field of a Spinning Mass as an Example of Algebraically Special Metrics. *Phys. Rev. Lett.*, 11(5):237–238, Sep 1963. <https://doi.org/10.1103/PhysRevLett.11.237>.
- S. M. Kopeikin, M. Efroimsky, and G. Kaplan. *Relativistic Celestial Mechanics of the Solar System*. Wiley-VCH, Weinheim, Aug 2011. <https://doi.org/10.1002/9783527634569>.
- H. Korth, R. Pappalardo, K. Craft, I. Daubar, H. Hay, S. Howell, R. Klima, E. Leonard, A. Matiella Novak, D. Persaud, and C. Phillips. Europa Clipper Mission Update. In *EGU General Assembly Conference Abstracts*, EGU General Assembly Conference Abstracts, pages EGU22–6052, May 2022. <https://doi.org/10.5194/egusphere-egu22-6052>.
- M. Kramer, I. H. Stairs, R. N. Manchester, M. A. McLaughlin, A. G. Lyne, R. D. Ferdman, M. Burgay, D. R. Lorimer, A. Possenti, N. D’Amico, J. M. Sarkissian, G. B. Hobbs, J. E. Reynolds, P. C. C. Freire, and F. Camilo. Tests of General Relativity from Timing the Double Pulsar. *Science*, 314:97–102, Oct 2006. <https://doi.org/10.1126/science.1132305>.
- U. J. Le Verrier. Lettre de M. Le Verrier à M. Faye sur la théorie de Mercure et sur le mouvement du périhélie de cette planète. *Cr. Hebd. Acad. Sci.*, 49: 379–383, Aug 1859.
- J. Lense and H. Thirring. Über den Einfluß der Eigenrotation der Zentralkörper auf die Bewegung der Planeten und Monde nach der Einsteinschen Gravitationstheorie. *Phys. Z.*, 19:156–163, 1918.
- D. M. Lucchesi and R. Peron. Accurate Measurement in the Field of the Earth of the General-Relativistic Precession of the LAGEOS II Pericenter and New Constraints on Non-Newtonian Gravity. *Phys. Rev. Lett.*, 105(23):231103, Dec 2010. <https://doi.org/10.1103/PhysRevLett.105.231103>.
- D. M. Lucchesi and R. Peron. LAGEOS II pericenter general relativistic precession (1993-2005): Error budget and constraints in gravitational physics. *Phys. Rev. D*, 89(8):082002, Apr 2014. <https://doi.org/10.1103/PhysRevD.89.082002>.
- D. M. Lucchesi, M. Visco, R. Peron, M. Bassan, G. Pucacco, C. Pardini, L. Anselmo, and C. Magnafico. A 1% Measurement of the Gravitomagnetic Field of the Earth with Laser-Tracked Satellites. *Universe*, 6(9):139, Aug 2020. <https://doi.org/10.3390/universe6090139>.
- A. Magnanini. Estimation of the Ephemerides and Gravity Fields of the Galilean Moons Through Orbit Determination of the JUICE Mission. *Aerotec. Missili Spaz.*, 100(3):195–206, Sep 2021. <https://doi.org/10.1007/s42496-021-00090-6>.
- B. Mashhoon. Gravitational couplings of intrinsic spin. *Class. Quantum Grav.*, 17(12):2399–2409, Jun 2000. <https://doi.org/10.1088/0264-9381/17/12/312>.
- B. Mashhoon, F. W. Hehl, and D. S. Theiss. On the gravitational effects of rotating masses: the Thirring-Lense papers. *Gen. Relativ. Gravit.*, 16(8):711–750, Aug 1984. <https://doi.org/10.1007/BF00762913>.
- S. Matousek. The Juno New Frontiers mission. *Acta Astronaut.*, 61(10):932–939, Nov 2007. <https://doi.org/10.1016/j.actaastro.2006.12.013>.
- B. H. Mauk. Comparative investigation of the energetic ion spectra comprising the magnetospheric ring currents of the solar system. *J. Geophys. Res. Space Phys.*, 119(12):9729–9746, Dec 2014. <https://doi.org/10.1002/2014JA020392>.
- B. H. Mauk and N. J. Fox. Electron radiation belts of the solar system. *J. Geophys. Res. Space Phys.*, 115(A12):A12220, Dec 2010. <https://doi.org/10.1029/2010JA015660>.
- J. Meichsner and M. H. Soffel. Effects on satellite orbits in the gravitational field of an axisymmetric central body with a mass monopole and arbitrary spin multipole moments. *Celest. Mech. Dyn. Astr.*, 123(1):1–12, Sep 2015. <https://doi.org/10.1007/s10569-015-9626-3>.
- O. Montenbruck and E. Gill. *Satellite Orbits*. Springer-Verlag, Berlin Heidelberg, Jun 2000. <https://doi.org/10.1007/978-3-642-58351-3>.
- N. Mouawad, A. Eckart, S. Pfalzner, R. Schödel, J. Moutkaka, and R. Spurzem. Weighing the cusp at the Galactic Centre. *Astron. Nachr.*, 326(2):83–95, Feb 2005. <https://doi.org/10.1002/asna.200410351>.
- T. D. Moyer. *Formulation for Observed and Computed Values of Deep Space Network Data Types for Navigation*. JPL Deep Space Communications and Navigation Series. Wiley-Interscience, Hoboken, New Jersey, Jan 2003. <https://doi.org/10.1002/0471728470>.
- A. M. Nobili and C. M. Will. The real value of Mercury’s perihelion advance. *Nature*, 320:39–41, Mar 1986. <https://doi.org/10.1038/320039a0>.
- A. A. Nucita, F. De Paolis, G. Ingrosso, A. Qadir, and A. F. Zakharov. Sgr A*: A Laboratory to Measure the Central Black Hole and Stellar Cluster Parameters. *Publ. Astron. Soc. Pac.*, 119(854):349–359, Apr 2007. <https://doi.org/10.1086/517934>.
- M. Panhans and M. H. Soffel. Gravitomagnetism of an extended celestial body. *Class. Quantum Grav.*, 31(24):245012, Dec 2014. <https://doi.org/10.1088/0264-9381/31/24/245012>.
- F. Peißker, A. Eckart, M. Zajaček, B. Ali, and M. Parsa. S62 and S4711: Indications of a Population of Faint Fast-moving Stars inside the S2 Orbit—S4711 on a 7.6 yr Orbit around Sgr A*. *Astrophys. J.*, 899(1):50, Aug 2020. <https://doi.org/10.3847/1538-4357/ab9c1c>.
- F. Peißker, A. Eckart, M. Zajaček, and S. Britzen. Observation of S4716-a Star with a 4 yr Orbit around Sgr A*. *Astrophys. J.*, 933(1):49, Jul 2022. <https://doi.org/10.3847/1538-4357/ac752f>.
- G. Petit and B. Luzum, editors. *IERS Conventions (2010)*, volume 36 of *IERS Technical Note*. Verlag des Bundesamts für Kartographie und Geodäsie, Frankfurt am Main, 2010.
- E. Poisson and C. M. Will. *Gravity*. Cambridge University Press, Cambridge, Jun 2014. <https://doi.org/10.1017/CBO9781139507486>.
- G. E. Pugh. Proposal for a Satellite Test of the Coriolis Prediction of General Relativity. Research Memorandum 11, Weapons Systems Evaluation Group, The Pentagon, Washington D.C., Nov 1959.
- G. Renzetti. History of the attempts to measure orbital frame-dragging with artificial satellites. *Centr. Eur. J. Phys.*, 11(5):531–544, Jul 2013. <https://doi.org/10.2478/s11534-013-0189-1>.
- D. C. Robinson. Uniqueness of the Kerr Black Hole. *Phys. Rev. Lett.*, 34(14):905–906, Apr 1975. <https://doi.org/10.1103/PhysRevLett.34.905>.
- E. Roussos, O. Allanson, N. André, B. Bertucci, G. Branduardi-Raymont, G. Clark, K. Dialynas, I. Dandouras, R. T. Desai, Y. Futaana, M. Gkioulidou, G. H. Jones, P. Kollmann, A. Kotova, E. A. Kronberg, N. Krupp, G. Murakami, Q. Nénon, T. Nordheim, B. Palmaerts, C. Plainaki, J. Rae, D. Santos-Costa, T. Sarris, Y. Shprits, A. Sulaiman, E. Woodfield, X. Wu, and Z. Yao. The in-situ exploration of Jupiter’s radiation belts. *Exp. Astron.*, 54(2-3):745–789, Oct 2022. <https://doi.org/10.1007/s10686-021-09801-0>.
- G. F. Rubilar and A. Eckart. Periastron shifts of stellar orbits near the Galactic Center. *Astron. Astrophys.*, 374:95–104, Jul 2001. <https://doi.org/10.1051/0004-6361/20010640>.
- M. Schanner and M. H. Soffel. Relativistic satellite orbits: central body with higher zonal harmonics. *Celest. Mech. Dyn. Astr.*, 130(6):40, Jun 2018. <https://doi.org/10.1007/s10569-018-9836-6>.
- A. Schärer, R. Bondarescu, P. Saha, R. Angélic, R. Helled, and P. Jetzer. Prospects for Measuring Planetary Spin and Frame-Dragging in Spacecraft Timing Signals. *Front. Astron. Space Sci.*, 4:11, Sep 2017. <https://doi.org/10.3389/fspas.2017.00011>.
- L. Schiff. Possible new experimental test of general relativity theory. *Phys. Rev. Lett.*, 4(5):215–217, Mar 1960. <https://doi.org/10.1103/PhysRevLett.4.215>.
- P. K. Seidelmann, B. A. Archinal, M. F. A’Hearn, A. Conrad, G. J. Consolmagno, D. Hestroffer, J. L. Hilton, G. A. Krasinsky, G. Neumann, J. Oberst, P. Stooke, E. F. Tedesco, D. J. Tholen, P. C. Thomas, and I. P. Williams. Report of the IAU/IAG Working Group on cartographic coordinates and rotational elements: 2006. *Celest. Mech. Dyn. Astr.*, 98(3):155–180, Jul 2007. <https://doi.org/10.1007/s10569-007-9072-y>.
- I. I. Shapiro. Solar system tests of general relativity: recent results and present plans. In N. Ashby, D. F. Bartlett, and W. Wyss, editors, *General Relativity and Gravitation, 1989*, pages 313–330. Cambridge University Press, Cambridge, Nov 1990. <https://doi.org/10.1017/CBO9780511564178.025>.

- I. I. Shapiro, M. E. Ash, and W. B. Smith. Icarus: Further Confirmation of the Relativistic Perihelion Precession. *Phys. Rev. Lett.*, 20:1517–1518, Jun 1968. <https://doi.org/10.1103/PhysRevLett.20.1517>.
- I. I. Shapiro, W. B. Smith, M. E. Ash, and S. Herrick. General Relativity and the Orbit of Icarus. *Astron J.*, 76:588, Sep 1971. <https://doi.org/10.1086/111168>.
- I. I. Shapiro, G. H. Pettengill, M. E. Ash, R. P. Ingalls, D. B. Campbell, and R. B. Dyce. Mercury’s Perihelion Advance: Determination by Radar. *Phys. Rev. Lett.*, 28:1594–1597, Jun 1972. <https://doi.org/10.1103/PhysRevLett.28.1594>.
- M. H. Soffel. *Relativity in Astrometry, Celestial Mechanics and Geodesy*. Springer, Heidelberg, 1989. <https://doi.org/10.1007/978-3-642-73406-9>.
- M. H. Soffel and W.-B. Han. *Applied General Relativity*. Astronomy and Astrophysics Library. Springer Nature Switzerland, Cham, Oct 2019. <https://doi.org/10.1007/978-3-030-19673-8>.
- M. H. Soffel, R. Wirrer, J. Schastok, H. Ruder, and M. Schneider. Relativistic Effects in the Motion of Artificial Satellites - the Oblateness of the Central Body I. *Celest. Mech. Dyn. Astr.*, 42(1-4):81–89, Mar 1987. <https://doi.org/10.1007/BF01232949>.
- M. H. Soffel, S. A. Klioner, G. Petit, P. Wolf, S. M. Kopeikin, P. Bretagnon, V. A. Brumberg, N. Capitaine, T. Damour, T. Fukushima, B. Guinot, T. Y. Huang, L. Lindegren, C. Ma, K. Nordtvedt, J. C. Ries, P. K. Seidelmann, D. Vokrouhlický, C. M. Will, and C. Xu. The IAU 2000 Resolutions for Astrometry, Celestial Mechanics, and Metrology in the Relativistic Framework: Explanatory Supplement. *Astron J.*, 126(6):2687–2706, Dec 2003. <https://doi.org/10.1086/378162>.
- A. Tartaglia. Detection of the gravitomagnetic clock effect. *Class. Quantum Gravit.*, 17(4):783–792, Feb 2000a. <https://doi.org/10.1088/0264-9381/17/4/304>.
- A. Tartaglia. Influence of the angular momentum of astrophysical objects on light and clocks and related measurements. *Class. Quantum Gravit.*, 17(12): 2381–2384, Jun 2000b. <https://doi.org/10.1088/0264-9381/17/12/310>.
- S. A. Teukolsky. The Kerr metric. *Class. Quantum Gravit.*, 32(12):124006, Jun 2015. <https://doi.org/10.1088/0264-9381/32/12/124006>.
- C. M. Will. Incorporating post-Newtonian effects in N-body dynamics. *Phys. Rev. D*, 89(4):044043, Feb 2014. <https://doi.org/10.1103/PhysRevD.89.044043>.
- A. F. Zakharov, A. A. Nucita, F. de Paolis, and G. Ingrosso. Apoastron shift constraints on dark matter distribution at the Galactic Center. *Phys. Rev. D*, 76(6): 062001, Sep 2007. <https://doi.org/10.1103/PhysRevD.76.062001>.